NASA TECHNICAL NOTE

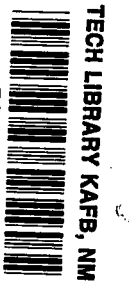

NASA TN D-7046

EXPERIMENTAL AERODYNAMIC PERFORMANCE CHARACTERISTICS OF A ROTOR ENTRY VEHICLE CONFIGURATION

I – Subsonic

by Ronald C. Smith and Alan D. Levin

Ames Research Center
Moffett Field, Calif. 94035

NATIONAL AERONAUTICS AND SPACE ADMINISTRATION • WASHINGTON, D. C. • FEBRUARY 1971

1. Report No. NASA TN D-7046	2. Government Accession No.	3.
4. Title and Subtitle EXPERIMENTAL AERODYNAMIC PERFORMANCE CHARACTERISTICS OF A ROTOR ENTRY VEHICLE CONFIGURATION I – SUBSONIC		5. Report Date February 1971 6. Performing Organization Code
7. Author(s) Ronald C. Smith and Alan D. Levin		8. Performing Organization Report No. A - 3709
9. Performing Organization Name and Address NASA Ames Research Center Moffett Field, Calif., 94035		10. Work Unit No. 124-07-11-11-00-21 11. Contract or Grant No.
12. Sponsoring Agency Name and Address National Aeronautics and Space Administration Washington, D. C., 20546		13. Type of Report and Period Covered Technical Note 14. Sponsoring Agency Code
15. Supplementary Notes		

16. Abstract

Wind-tunnel tests were conducted to determine the aerodynamic performance characteristics of an unpowered rotor entry vehicle configuration at Mach numbers of 0.3 and 0.7. Rotor blade configurations having double wedge and modified ellipse profiles were tested at vehicle angles of attack from 15° to 90°. The ellipse profile was tested for rotor diameters of 45 and 60 inches. Variable blade collective pitch was used to control rotor rotational speed.

It was found that the rotor had an unstable operating range at tunnel speeds up to $M_\infty = 0.3$ for the low-angle glide attitudes. At higher speeds, manual control of rotor RPM was simple and straightforward. Test results indicate that the rotor produced destabilizing pitching moments putting the test configuration out of longitudinal trim in glide attitude. At $M_\infty = 0.3$ the maximum lift-drag ratio was about 2.6 for the long-blade configuration, and 1.8 for both short-blade configurations. At $M_\infty = 0.7$ the maximum lift-drag ratio was 1.1 for all the test configurations.

17. Key Words (Suggested by Author(s)) Entry Vehicles Rotor Performance Rotor Aerodynamics Autorotating Rotor Characteristics Subsonic	18. Distribution Statement Unclassified – Unlimited	

19. Security Classif. (of this report)	20. Security Classif. (of this page)	21. No. of Pages	22. Price*
Unclassified	Unclassified	40	$3.00

*For sale by the National Technical Information Service, Springfield, Virginia 22151

NOTATION

The body axes, force and moment coefficients, and angles used are shown in figure 1.

b	number of blades
c	blade chord
C_D	drag coefficient, $\frac{\text{drag}}{q_\infty S}$
C_L	lift coefficient, $\frac{\text{lift}}{q_\infty S}$
C_l	body axis rolling-moment coefficient, $\frac{\text{rolling moment}}{q_\infty S d}$
C_m	pitching-moment coefficient, $\frac{\text{pitching moment}}{q_\infty S d}$
C_N	normal-force coefficient, $\frac{\text{normal force}}{q_\infty S}$
C_X	axial-force coefficient, $\frac{\text{axial force}}{q_\infty S}$
C_Y	side-force coefficient, $\frac{\text{side force}}{q_\infty S}$
d	capsule diameter
$\frac{L}{D}$	lift-drag ratio
M_∞	free-stream Mach number
q_∞	free-stream dynamic pressure
R	rotor-blade radius measured normal to the axis of rotation with the blades in the fully open ($\beta = 0°$) position
R_{LE}	blade section leading-edge radius
S	capsule reference area, $\frac{\pi d^2}{4}$
V_∞	free-stream velocity

$\frac{\Omega R}{V_\infty}$	dimensionless tip speed
α	angle of attack, angle between relative wind and a plane normal to the shaft axis
β	flapping angle
θ_o	collective pitch angle
σ	rotor solidity, $\frac{bc}{\pi R}$
ψ	blade azimuth angle
Ω	rotor angular velocity

EXPERIMENTAL AERODYNAMIC PERFORMANCE CHARACTERISTICS OF A ROTOR ENTRY VEHICLE CONFIGURATION

I - SUBSONIC

Ronald C. Smith and Alan D. Levin

Ames Research Center

SUMMARY

Wind-tunnel tests have been conducted on several configurations of a rotor entry vehicle model to establish unpowered rotor operating characteristics at Mach numbers from 0.1 to 0.7 and to determine aerodynamic characteristics at Mach numbers 0.3 and 0.7. Tests were made using two different blade sections, a 20-percent modified ellipse and a 20-percent double-wedge, and two different blade lengths for the elliptic section. The three different rotor blade configurations were tested at vehicle angles of attack from 15° to 90° using variations in blade collective pitch angle to control rotor rotational speed.

It was found that the rotor had an unstable operating range at tunnel speeds up to and including $M_\infty = 0.3$ for the low-angle glide attitudes. At higher speeds, manual control of rotor RPM was simple and straightforward. Test results indicate that the rotor produced destabilizing pitching moments putting the test configurations out of longitudinal trim in glide attitude. At $M_\infty = 0.3$ the maximum lift-drag ratio was about 2.6 for the long-blade configuration, and 1.8 for both short-blade configurations. At $M_\infty = 0.7$ the maximum lift-drag ratio was 1.1 for all the test configurations.

INTRODUCTION

As the recovery of instrumented and manned space capsules becomes more frequent, the need for a recovery system that can provide a safe landing almost anywhere and in adverse weather becomes more urgent. While parachutes, paragliders, and lifting bodies can perform certain missions, none of these recovery systems has the operational flexibility needed to perform a large variety of recovery missions.

One system that appears to possess the desired capabilities is the deployable autorotating rotor. Specifically, the rotor offers the capability of (1) zero speed touchdown; (2) touchdown at an unprepared landing site; and (3) aerodynamic force modulation without changes in the vehicle's attitude. The idea of using a rotor for lift and retardation during recovery from orbit is not new and has been investigated and reported by various authors (see refs. 1-5).

The investigation reported herein is part of a program designed to determine the feasibility of using an autorotating rotor for lift and drag modulation from orbital speed to touchdown. An analytical study has been made to estimate the aerodynamic characteristics of a rotor entry vehicle

(REV) configuration and to determine its performance as an entry vehicle. This work has been reported in reference 6. The entry performance study indicated that the REV could provide substantial range capability if the aerodynamic heating of the rotor blades would not severely restrict the flight envelope. In order to establish the limits on velocity and altitude imposed by blade heating, experiments were made on a small REV model in the Ames 1-foot shock tunnel to measure blade heating rates (ref. 7). The results agree favorably with heating estimates for near-axial flight (flight nearly parallel to rotor axis) and indicate that the rotor can be used for retardation during the entire entry. Blade-leading-edge heating rates measured in glide flight were not valid because of the small size of the model. Heating rates estimated for the leading edge indicate that the rotor can be utilized in glide flight (15° to 28.5° angle of attack) at speeds below about 16,000 feet per second (200,000 ft altitude) if the blade is radiation-cooled and has a ceramic coating capable of withstanding 3700° F. The study reported in reference 6 indicated that delaying glide flight until a speed of 16,000 feet per second is reached would reduce lateral range from 650 statute miles (glide flight from orbit) to about 500 statute miles.

Unfortunately, work on rotor systems to date was either theoretical or limited to tests at near-axial attitudes for high forward speeds. Hence, very little was known about the aerodynamic and operating characteristics (rotational speed versus blade pitch) of rotors in high speed glide flight.

The objectives of the experimental test program, of which this report is a part, are to provide experimental rotor operating (RPM vs blade pitch) and aerodynamic characteristics to substantiate the entry performance of an REV as well as to add substantially to the knowledge of high speed unpowered rotors. Accordingly, a wind-tunnel model of an REV configuration was built and successfully tested at Mach numbers up to 3.5 at angles of attack from 15° to 90°.

Because of the lack of information on operating characteristics of unpowered rotors in the proposed speed range, tunnel speed was increased gradually in the initial tests. In order to approximate rotor-alone characteristics, these tests were made at $\alpha = 90°$ with a cone forebody in place of the entry vehicle body. These tests revealed instabilities in rotor rotational speed at Mach numbers between 0.1 and 0.4 and the results are included herein.

This report is the first part of a three-part series covering the three speed regimes tested. Parts II and III cover the transonic and supersonic speed regimes, respectively. Table 1 indicates the scope of the experimental investigation to determine aerodynamic characteristics of the entry vehicle (body-rotor) configuration.

MODEL DESCRIPTION

The rotor entry vehicle model tested is a four-bladed rotor mounted on a capsule body. The mechanical design and fabrication were performed by the Kaman Aircraft Corporation according to general specifications provided by Ames Research Center. Detailed drawings of the model are shown in figure 2. The model is shown mounted in the Ames 12-Foot Pressure Wind Tunnel in figure 3.

Rotor

The rotor blades have variable collective pitch and were allowed to flap about offset flapping hinges within predetermined limits; however, they do not have lead-lag freedom. Collective pitch could be changed remotely by means of a conventional swash plate. The total range of collective pitch travel is ±90° but only a 40° range is available through the use of the remote control system. The blades could be attached at 15° increments, which allowed the entire collective pitch range to be tested. The design operating tip speed is 1100 ft/sec. A detailed description of the model, control system features, and strength requirements can be found in reference 8.

Blades

Two different blade airfoil sections, a modified ellipse and a double wedge, were tested and are illustrated in figure 2(b). Blades having the modified ellipse section were tested in two blade lengths which gave rotor diameters of 45 and 60 inches corresponding to solidities of 20 and 15 percent, respectively. The double-wedge section was used only with the smaller rotor diameter. The maximum thickness-to-chord ratio is 0.20. The rotor blades are untwisted and have a rectangular planform. They were fabricated of a fiberglass epoxy laminate with most of the fibers oriented in the spanwise (radial) direction, giving the blades an extremely high strength-to-weight ratio in the radial direction.

Forebodies

The capsule body is a typical blunt entry vehicle consisting of a body of revolution about the rotor axis. Its geometry is shown in figure 2(a). The maximum diameter of the body is 15 inches, which gives rotor-to-capsule diameter ratios of 3 and 4 for the 45- and 60-inch-diameter rotors, respectively. The cone-cylinder forebody, used in place of the capsule body to simulate rotor-alone operating characteristics, is shown in figure 2(c).

Model Mounting Details

In order to cover the angle-of-attack range from 0° to 90°, three different model mounting arrangements were utilized. In all cases the balance centerline was coincident with the rotor axis as shown in figure 4. For the angle-of-attack range from 0° to 28.5° (fig. 4(a)), the model and balance were mounted on a 90° elbow attached to the model support sting. In the range from 31.5° to 60° (fig. 4(b)) the model and balance were mounted on a 30° bent adapter attached to the sting. In the range from 61.5° to 90° (fig. 4(c)) the model and balance were mounted in line with the sting. For the angle-of-attack range from 31.5° to 90° the wind-tunnel support system necessitated mounting the model upside down. For this range of angles of attack the model lift was positive in the downward direction.

Flapping stop- For the angle-of-attack range from 0° to 28.5° a flapping stop (fig. 2(a)) was mounted on the rotor hub to prevent large flapping excursions of the rotor blades when the tunnel was started and when conditions that cause flapping instability occurred during the testing. This stop held

flapping to 20°. When the model was mounted in the 31.5° to 60° attitude, a flapping stop was also required to prevent the rotor blades from striking the support sting. This flapping stop allowed up to 45° of flapping freedom. For tests in the axial configuration, the flapping stop was removed.

Blade cager (axial mounting only)- A blade caging arrangement (fig. 5) held the blades in a stowed position along the support sting during the tunnel starting operation. The cager could be used only when the model was mounted in the axial ($\alpha = 90°$) configuration. After the data were taken, the rotor could be stopped and re-caged before the tunnel was shut down. The caging mechanism was equipped to provide remote opening and closing.

INSTRUMENTATION AND TEST PROCEDURE

Instrumentation

The model forces were measured by means of a 1.75-inch 6-component internal strain gage balance. Rotor RPM was obtained from two magnetic pickups mounted on the stationary swash plate inside the model. The magnetic pickups were energized by the passage of teeth on the rotating swashplate producing an a.c. output at the tooth-passing frequency. A gap left by the omission of one tooth produces a gap in the harmonic output of each of the magnetic pickups. These gaps in the outputs when viewed simultaneously on a dual-beam oscilloscope allowed determination of the direction of rotation.

Test Procedure

In the axial flow tests ($\alpha = 90°$), the blades were folded back along the sting and held by the cager. After the tunnel reached test conditions, the cager was opened to allow deployment of the rotor. Both collective pitch and cyclic pitch were used to initiate the deployment, which simulated deployment during the recovery process. Before the tunnel was shut down, the rotor was stopped by setting the blade pitch at zero. Under these conditions the flow forces the blades back along the sting. Finally, the blades were clamped in place by closing the cager. This procedure minimized the possibility of damaging the rotor during the tunnel shutdown operations. At low and intermediate angles of attack, rotor rotation was initiated at a free-stream dynamic pressure of about 50 psf by use of the collective pitch control.

In the glide attitude ($\alpha = 15°$ to $28.5°$) it was found to be "unsafe" to operate the rotor at angles of attack less than 15° because of flapping instability. This instability occurs when there is insufficient centrifugal force to generate the required moment about the flapping hinge to balance the aerodynamic moment. The resulting flapping excursions can easily cause blade failure by repeatedly contacting the blade grip with the flapping stop.

The investigation was conducted by parametrically varying the blade collective pitch angle at fixed conditions of free-stream Mach number and angle of attack. Throughout the tests the model was maintained at zero sideslip angle. Rotor rotation was always clockwise when viewed from the top.

WIND TUNNEL, TEST CONDITIONS AND DATA ACCURACY

The tests were conducted in the Ames 12-Foot Pressure Wind Tunnel which is a variable-density, low-turbulence subsonic facility. The highest Mach number obtainable with the rotor model mounted in the maximum-drag attitude was about 0.8.

Aerodynamic characteristics were determined at a total pressure of 5 in. Hq (354 psf) which was held constant throughout these tests. For the two Mach numbers used to study the model aerodynamic characteristics, the dynamic pressure and Reynolds number based on capsule diameter were as follows:

Mach number	Dynamic pressure, psf	Reynolds number
0.3	21	0.40×10^6
0.7	91	0.71×10^6

Rotor operating characteristics at Mach numbers of 0.2 and below were determined at a total pressure of 1 atmosphere.

The balance used for these tests was sized for later use at dynamic pressures up to 500 psf at a Mach number of 1.4. The dynamic pressures of the present tests produced loads no greater than about 4 percent of balance capacity at $M_\infty = 0.3$ and 15 percent capacity at $M_\infty = 0.7$. The maximum uncertainties in the data are estimated to be as follows:

Coefficient	$M_\infty = 0.3$	$M_\infty = 0.7$
C_l	±0.025	±0.006
C_m	±0.05	±0.01
C_D	±0.15	±0.035
C_L	±0.25	±0.06
C_Y	±0.22	±0.05
L/D	±0.3	±0.06
M_∞	±0.005	±0.005
$\Omega R/V_\infty$	±0.01	±0.003
α	±0.1°	±0.1°
θ_o	±0.25°	±0.25°

In general, repeatability of the force data was well within the maximum uncertainties indicated.

RESULTS AND DISCUSSION

The results of the tests reported herein are presented graphically in figures 6 through 13. The discussion of these results is divided into three sections: (1) rotor operating characteristics (RPM or $\Omega R/V_\infty$ vs θ_0), (2) body aerodynamic characteristics, and (3) body-plus-rotor aerodynamic characteristics.

Rotor Operating Characteristics

The effect of Mach number on the operating characteristics of the short elliptic-blade rotor with the cone forebody (fig. 2(c)) at $\alpha = 90°$ is illustrated in figure 6. At $M_\infty = 0.1$ the rotor sustains autoration for blade pitch angles up to about 5°. When the blade pitch was increased beyond 5°, blade stall caused the rotor to stop and cone back. The rotor then redeployed almost instantaneously with rotation in the opposite direction. At $M_\infty = 0.14$ and above, the rotor's operating range is confined to negative blade pitch angles. At $M_\infty = 0.2$ there are two stable operating ranges connected by an unstable transition region. The low RPM and high RPM ranges correspond to stalled and unstalled rotor operation, respectively. At $M_\infty = 0.2$, rotor speed data could be obtained in the unstable transition region provided the total pressure was no greater than one-fourth atmosphere. At such low total pressures, the response time of the rotor is sufficiently long to permit holding model rotation at unstable equilibrium. However, any slight disturbance would cause the rotor to seek a stable equilibrium condition, which for $\theta_0 = -4$ could be at either 700 or 4500 RPM. Above $M_\infty = 0.2$ the unstable operating characteristics have completely disappeared, although the slope of the curve is very steep. Thus at Mach numbers above 0.2 small changes in blade pitch produced large changes in rotor speed. Had the instabilities that occur at $M_\infty = 0.2$ and below persisted at higher Mach numbers, rotor speed control could become a serious problem.

The effect of angle of attack on the rotor speed characteristics for the short elliptic-blade rotor with capsule forebody is shown in figure 7. The rotor speed as a function of blade pitch angle for $M_\infty = 0.3$ is illustrated in figure 7(a). At $\alpha = 15°$ the rotor speed is essentially constant over a wide range of blade pitch angles. At low angles of attack the rotor was not permitted to operate at speeds below about 1000 RPM to avoid the possibility of the rotor blade grips repeatedly contacting the upper flapping stop. The rotor speed increases with angle of attack between $\alpha = 15°$ and $\alpha = 28.5°$. At $\alpha = 28.5°$ the rotor can be operated in either the stalled or unstalled state. Note the unstable operating range between -3° and -5° blade pitch angle. Above $\alpha = 28.5°$ rotor speed becomes very sensitive to changes in blade pitch angle over most of the range of blade pitch angles investigated. At $M_\infty = 0.7$ the variation of operating characteristics are markedly different from those at $M_\infty = 0.3$. At $M_\infty = 0.7$ the variation of rotor speed with changes in blade pitch angle is smooth. As the angle of attack is reduced from 90° the rotor speed is less for a given blade pitch angle. At this Mach number the blades are completely stalled at nearly all vehicle angles of attack and therefore do not exhibit the transitional range between stalled and unstalled operation which characterizes low speed operation.

The effect of blade length on the rotor operating characteristics is presented in figure 8. The data presented are for the elliptic-blade section. The variation of the ratio of rotor tip-speed to free-stream velocity with blade pitch angle is presented for two angles of attack at $M_\infty = 0.3$

(fig. 8(a)) and $M_\infty = 0.7$ (fig. 8(b)). This parameter should, in the absence of body interference effects, be the same for rotors of any diameter and solidity. The theory of reference 6 indicates that at $\alpha = 90°$ the dimensionless tip speed should be a function only of the blade pitch angle and blade airfoil section. At both Mach numbers and angles of attack the long elliptic blades ran at higher tip speed, which suggests a body interference effect.

The dimensionless tip speed for the short elliptic and the double-wedge blade configurations are compared in figure 9. At $M_\infty = 0.3$ (fig. 9(a)), the double-wedge configuration has a much higher tip speed at $\alpha = 90°$ than the short elliptic blade. At $\alpha = 20°$ this trend is reversed. At $\alpha = 90°$ it is expected that the double-wedge configuration would have a higher tip speed than the elliptic blade as a result of a higher ratio of blade section normal force to chord force for the double-wedge section. At $\alpha = 20°$ both sections have about the same section normal force, but the elliptic blade has large negative chord force at low section angles of attack (ref. 9). Consequently, the elliptic-blade configuration has a substantially higher driving force and, hence, should exhibit higher tip speeds than the double-wedge configuration. At $M_\infty = 0.7$ (fig. 9(b)) the double-wedge section has a higher tip speed at both angles of attack, except for blade pitch angles less than $-8°$ at $\alpha = 20°$. Examination of blade section data in the range $M_\infty = 0.6–0.9$ (ref. 9) shows the double wedge to have a higher normal-force to chord-force ratio. It appears then that a qualitative comparison of rotor speed can be obtained from comparisons of blade section data.

Body Aerodynamic Characteristics

The longitudinal aerodynamic characteristics of the capsule forebody are presented in figure 10. The lift coefficient data for both Mach numbers exhibit a stall or a discontinuity between the test angles of attack 28.5° and 31.5°. It is not known whether this is caused by an aerodynamic phenomenon such as sting interference or by inaccuracy of force resolution. The moment center location for all configurations tested is as shown in figure 2(a). With this moment center location the body is stable at angles of attack between 40° and 90° and has a stable trim point at about 60°. The lift-drag ratio at the stable trim point is about 0.50.

Body-Plus-Rotor Aerodynamic Characteristics

The aerodynamic characteristics of the three body-rotor configurations tested have been plotted as functions of angle of attack for several blade pitch angles. The characteristics of the double-wedge blade configuration are presented in figure 11. The characteristics of the short and long elliptic-blade configurations are presented in figures 12 and 13, respectively. The force and moment data for $\alpha = 61.5°$ and 70° are not considered reliable because of apparent sting interference (see "Effects of sting inclination").

Longitudinal stability- At both test Mach numbers, all three body-rotor configurations generally have large positive pitching moments at all but the highest angles of attack; hence some powerful means of changing trim is needed. At $M_\infty = 0.3$, the pitching moment was quite sensitive to collective pitch in the intermediate α range, resulting in large changes in stability in that range. This sensitivity was not evident at $M_\infty = 0.7$. Longitudinal trim is indicated to occur at some angle of attack between 54° and 85°. The data for $\alpha = 61.5°$ and 70°, however, are not considered

reliable. Generally, the vehicle was stable at high angles of attack and neutrally stable or unstable at low angles. At $M_\infty = 0.3$, double values of pitching moment, as well as all other parameters, occur in the angle-of-attack range 25° to 50°. The two values correspond to rotor operation in the stalled and unstalled states.

Lift and drag- The rotor produced large increments in lift and drag that are roughly proportional to the rotor blade plan area for a given blade section. At $M_\infty = 0.3$, the short elliptic-blade configuration produced much higher lift than the double-wedge-blade configuration and accordingly had higher L/D. At $M_\infty = 0.7$ there is very little difference between any of the forces and moments for these two configurations. The lift and drag are relatively insensitive to changes in blade pitch angle at angles of attack below rotor stall ($\alpha \simeq 28°$) but become more sensitive as the angle of attack increases. At $M_\infty = 0.7$ the changes in lift and drag with blade pitch angle are much more orderly than at $M_\infty = 0.3$ where the effects of rotor stall have a dominant influence. In axial flight considerable modulation of the drag is available through variation of blade pitch angle. It is possible to reduce the drag to values much lower than indicated on the figures by slowing the rotor to allow very high coning angles. The lower limit of drag would be obtained by collapsing the rotor to give nearly the capsule-alone drag. Thus, the drag can be reduced to about 1/3 of its maximum value at $M_\infty = 0.7$ or about 1/5 at $M_\infty = 0.3$.

At $M_\infty = 0.3$ the maximum lift-drag ratio is about 1.8 for both short blade configurations and occurs at $\alpha = 20°$. For the long elliptic-blade configuration the maximum lift-drag ratio is about 2.6 and occurs at $\alpha = 15°$. At $M_\infty = 0.7$ the maximum lift-drag ratio is about 1.1 for all three configurations and occurs at $\alpha = 28.5°$.

Rolling moment and side force- Large rolling moments were produced at $M_\infty = 0.3$ by both elliptic-blade configurations at intermediate angles of attack. These rolling moments were twice as high as the corresponding pitching. moments. The double-wedge-blade configuration produced rolling moments which were somewhat smaller. At $M_\infty = 0.7$, the rolling moments are small for small negative blade pitch angles and increase in an orderly manner with increasingly negative blade pitch angle. At the higher negative blade pitch angles all three configurations have rolling moments larger than the corresponding pitching moments. Generally, these rolling moments were positive for clockwise rotor rotation (viewed from above). The rotor also produced substantial side force except for the $\alpha = 90°$ case. The side force was always negative and was greatest at $M_\infty = 0.3$.

Effect of sting inclination- Large discontinuities appear in the data between 60° and 61.5° angle of attack apparently as a result of differences in sting interference. The long elliptic-blade configuration appears most strongly affected. At $\alpha = 61.5°$, the sting inclination to the free stream was 28.5°. With the 30° bent balance adapter (fig. 4(b)) tests could be made at $\alpha = 60°$ with the sting parallel to the free stream. Therefore, the data at $\alpha = 60°$ are expected to be more reliable than the data at $\alpha = 61.5°$. Discontinuities also appear between the data for $\alpha = 28.5°$ and 31.5°. The differences in the model attachment point and the sting inclination with respect to the model probably caused most of the discontinuity. However, at $M_\infty = 0.3$ where the discontinuities are greatest, the data are multivalued (because of stalled rotor operation) which tends to mask the sting interference effects. Since the data for both $\alpha = 28.5°$ and 31.5° were taken with the same sting inclination to the free stream, neither can be thought of as being the more reliable.

CONCLUSIONS

Wind-tunnel tests have been made on several configurations of a rotor entry vehicle model to establish unpowered-rotor operating characteristics at Mach numbers from $M_\infty = 0.1$ to 0.7 and to determine aerodynamic characteristics at $M_\infty = 0.3$ and 0.7. The tests were made using two different blade sections, a 20-percent modified ellipse and a 20-percent double wedge, and two different blade lengths for the elliptic section. The two blade lengths gave rotor to body diameter ratios of 3.0 and 4.0. The double-wedge blades were in the shorter length. Blade collective pitch was used to control rotor speed at all model attitudes.

The results of these tests indicate the following conclusions:

1. The rotor had an unstable operating range at low tunnel speeds up to $M_\infty = 0.3$ inclusive. The instability disappeared as the stream speed was increased. At angle of attack $\alpha = 90°$ the instability persisted to just beyond $M_\infty = 0.2$. At $\alpha = 28.5°$ the instability persisted beyond $M_\infty = 0.3$.

2. For the two short blade rotor configurations, which differed only in blade cross section, the elliptic-blade configuration gave somewhat better lift characteristics at $M_\infty = 0.3$ than the double wedge blade configuration. At $M_\infty = 0.7$ there was little difference in any of the forces and moments.

3. The aerodynamic forces and moments were significantly affected by variations in blade pitch angle.

4. At low angles of attack the rotor produced large positive pitching moments for all three configurations tested. Generally, longitudinal trim is indicated at some angle of attack between 54° and 85°. All the vehicle configurations tested were stable at high angles of attack and neutrally stable or unstable at low angles.

5. The maximum lift-drag ratio was about 1.8 for the short blade configurations and about 2.6 for the long blade configuration at $M_\infty = 0.3$. These values occurred at angles of attack of 20° and 15°, respectively. At $M_\infty = 0.7$ the maximum L/D was about 1.1 for all three configurations tested and occurred at $\alpha = 28.5°$.

6. At $M_\infty = 0.3$ the rotor produced large rolling moments for both elliptic-blade configurations. These rolling moments were twice as high as the corresponding pitching moments. At $M_\infty = 0.7$ both short blade configurations produced only moderate maximum rolling moments.

Ames Research Center
National Aeronautics and Space Administration
Moffett Field, Calif., 94035, Sept. 15, 1970

REFERENCES

1. Haig, C. R., Jr.: The Use of Rotors for the Landing and Reentry Braking of Manned Spacecraft. IAS Paper No. 60-17, Jan. 1960.

2. Fletcher, C. J.; and Tesch, E. C., Jr.: ROR-Chute Concept for Recovery Systems. Thiokol Chemical Corp. TR 3740, Jan. 1961.

3. Kretz, M.: Application of Rotary Wing Techniques to Atmospheric Re-Entry and Launch Vehicle Recovery Problems. Paper presented at the European Symposium on Space Technology, London, England, June 1961.

4. Barzda, J. J.; and Schultz, E. R.: Test Results of Rotary-Wing Decelerator Feasibility Studies for Capsule Recovery Applications. SAE Paper No. 756D, Sept. 1963.

5. Ham, Norman D.: An Experimental and Theoretical Investigation of a Supersonic Rotating Decelerator. J. Am. Helicopter Soc., vol. 8 no. 1, Jan. 1963, pp. 8-18.

6. Levin, Alan D.; and Smith, Ronald C.: An Analytical Investigation of the Aerodynamic and Performance Characteristics of an Unpowered Rotor Entry Vehicle. NASA TN D-4537, 1968.

7. Smith, Ronald C.; and Levin, Alan D.: Heat Transfer Measurements on the Rotor Blade of a Rotor Entry Vehicle Model. NASA TN D-4065, 1967.

8. Hollrock, Richard: Final Report. Re-Entry Rotor Tested. Verti-Flite, Feb. 1967, pp. 31-32.

9. Randall, Greenfield A., Jr.: Aerodynamic Characteristics of two 20 Percent Thick, Rectangular Wings Up to 90° Angle of Attack at Subsonic, Transonic, and Supersonic Speeds. NASA CR-73097, 1967.

TABLE 1.- SCOPE OF THE BODY-ROTOR INVESTIGATION

	PART I		PART II		PART III	
Config. \ Mach No.	0.3	0.7	0.9	1.1	1.6	3.5
B	○	○	○	○	○	○
BR_d	○	○	○	○	○	○
$BR_e{}^L$	○	○	○	○		
BR_e	○	○	○	○	○	○

Configuration code:

B - Body

R_d - Short double-wedge blade section (R/d = 1.5)

$R_e{}^L$ - Long elliptic-blade section (R/d = 2.0)

R_e - Short elliptic-blade section (R/d = 1.5)

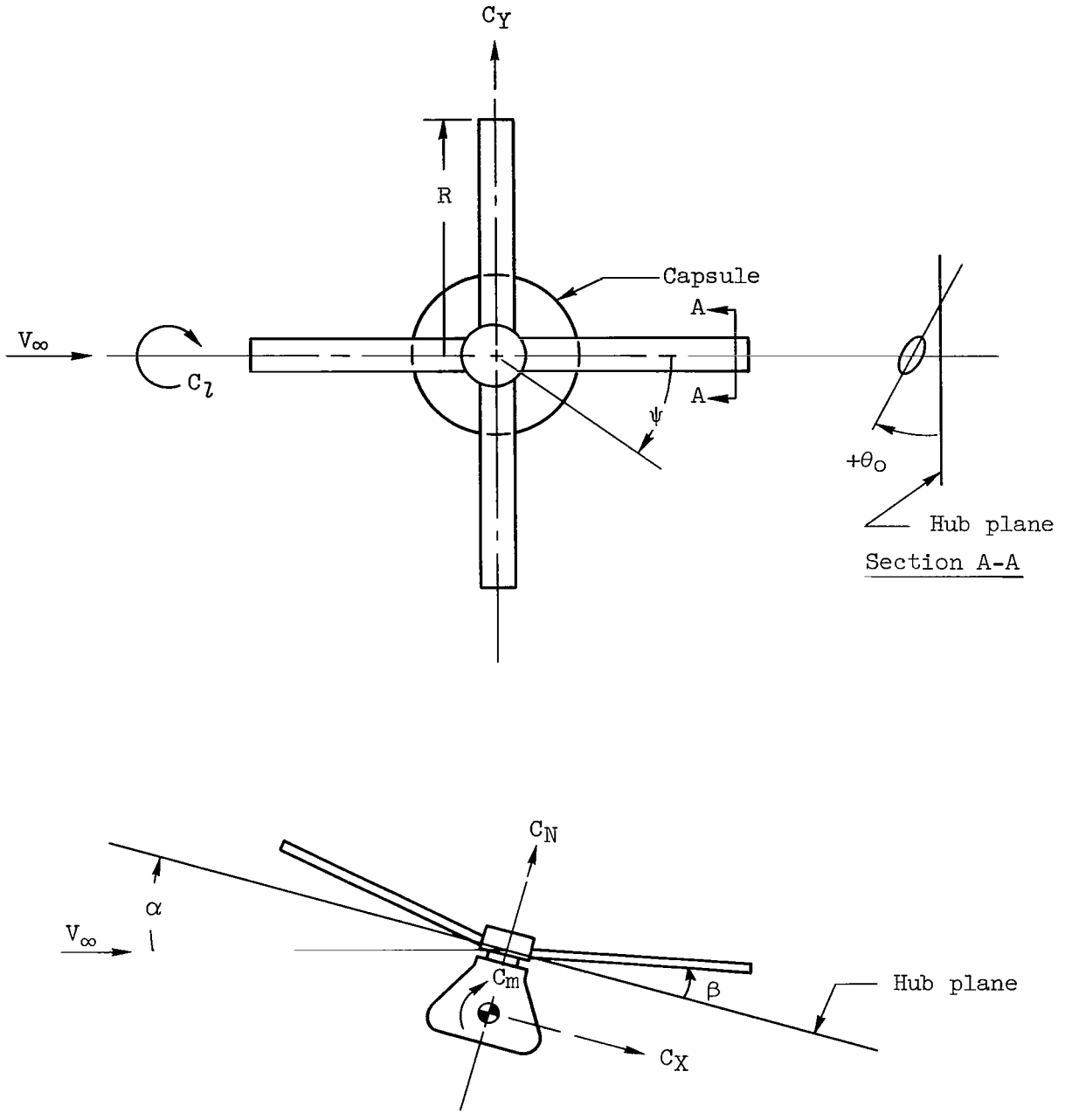

Figure 1.- Notation showing direction of forces and angles.

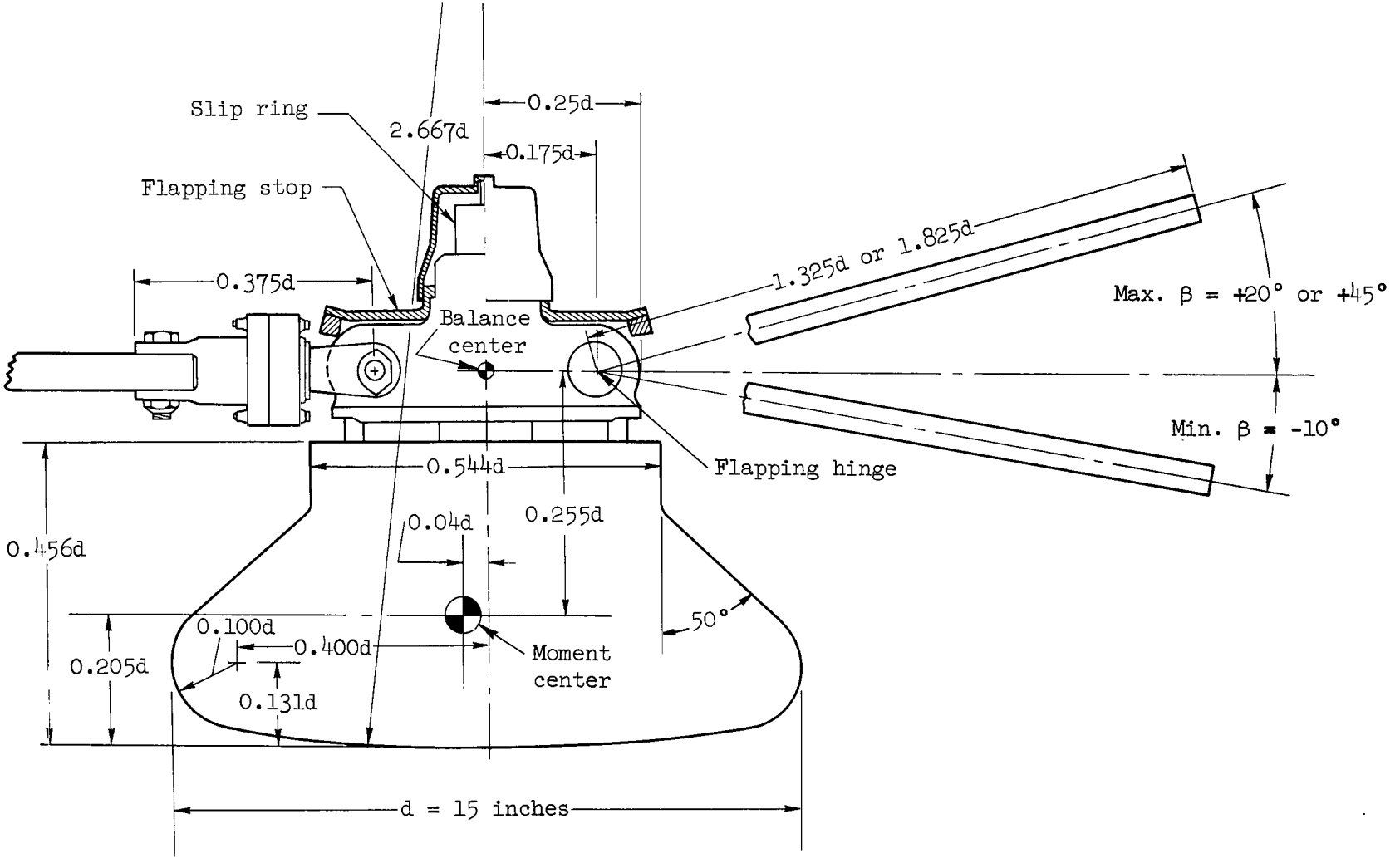

(a) Body and hub geometry

Figure 2.- Model details.

Note: All dimensions are in inches

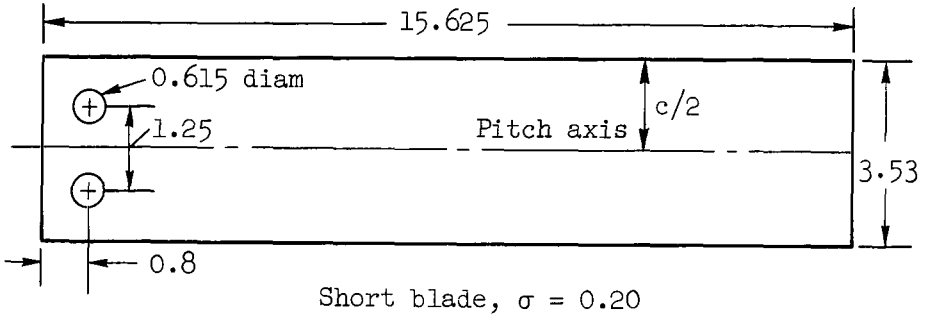

Short blade, $\sigma = 0.20$

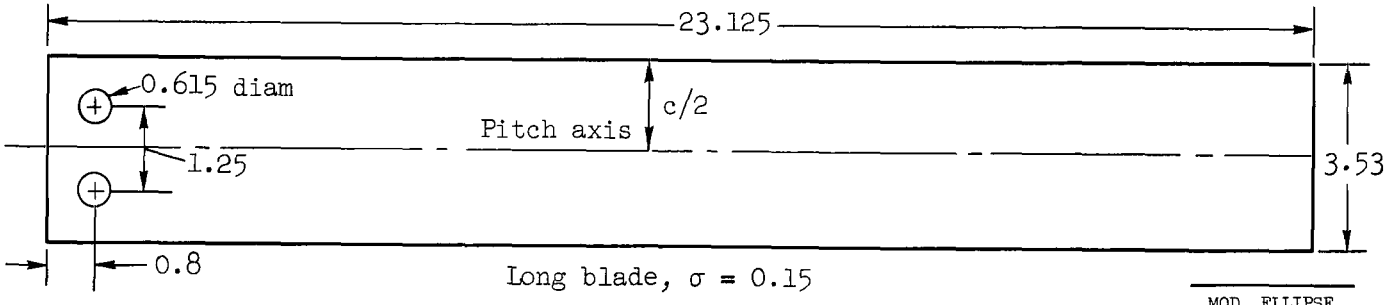

Long blade, $\sigma = 0.15$

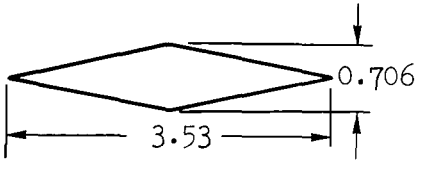

Wedge section

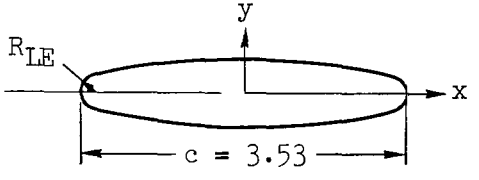

Modified ellipse section

$$\frac{R_{LE}}{c} = 0.0469$$

MOD. ELLIPSE COORDINATES	
± x/c	± y/c
0	0.1000
0.0417	0.0994
0.0834	0.0985
0.1250	0.0969
0.1667	0.0950
0.2083	0.0925
0.2500	0.0890
0.2917	0.0840
0.3333	0.0777
0.3750	0.0702
0.4167	0.0606
0.4583	0.0481
0.4688	0.0440
0.4792	0.0388
0.4896	0.0299

(b) Rotor blade geometry

Figure 2.- Continued.

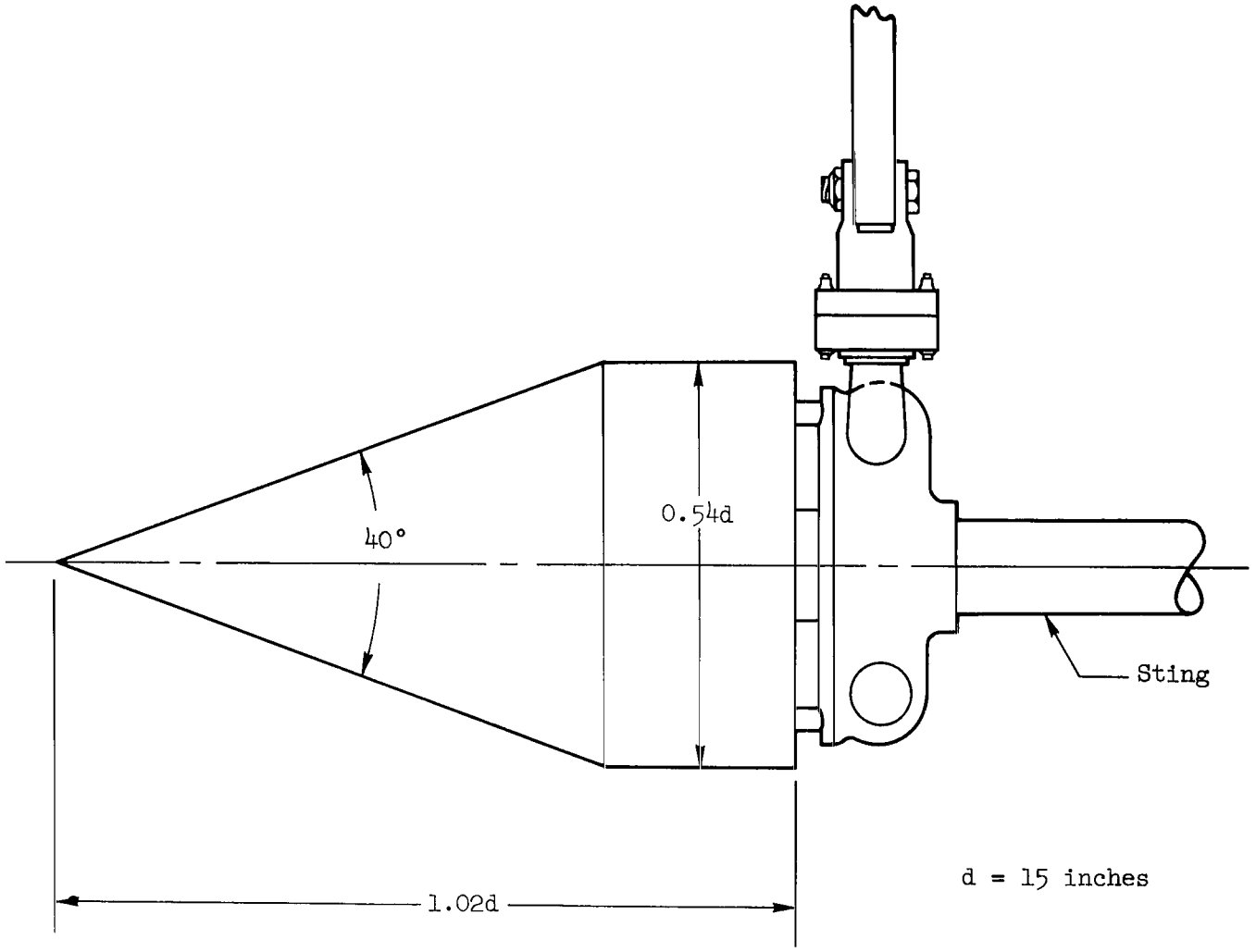

(c) Cone forebody geometry

Figure 2.- Concluded.

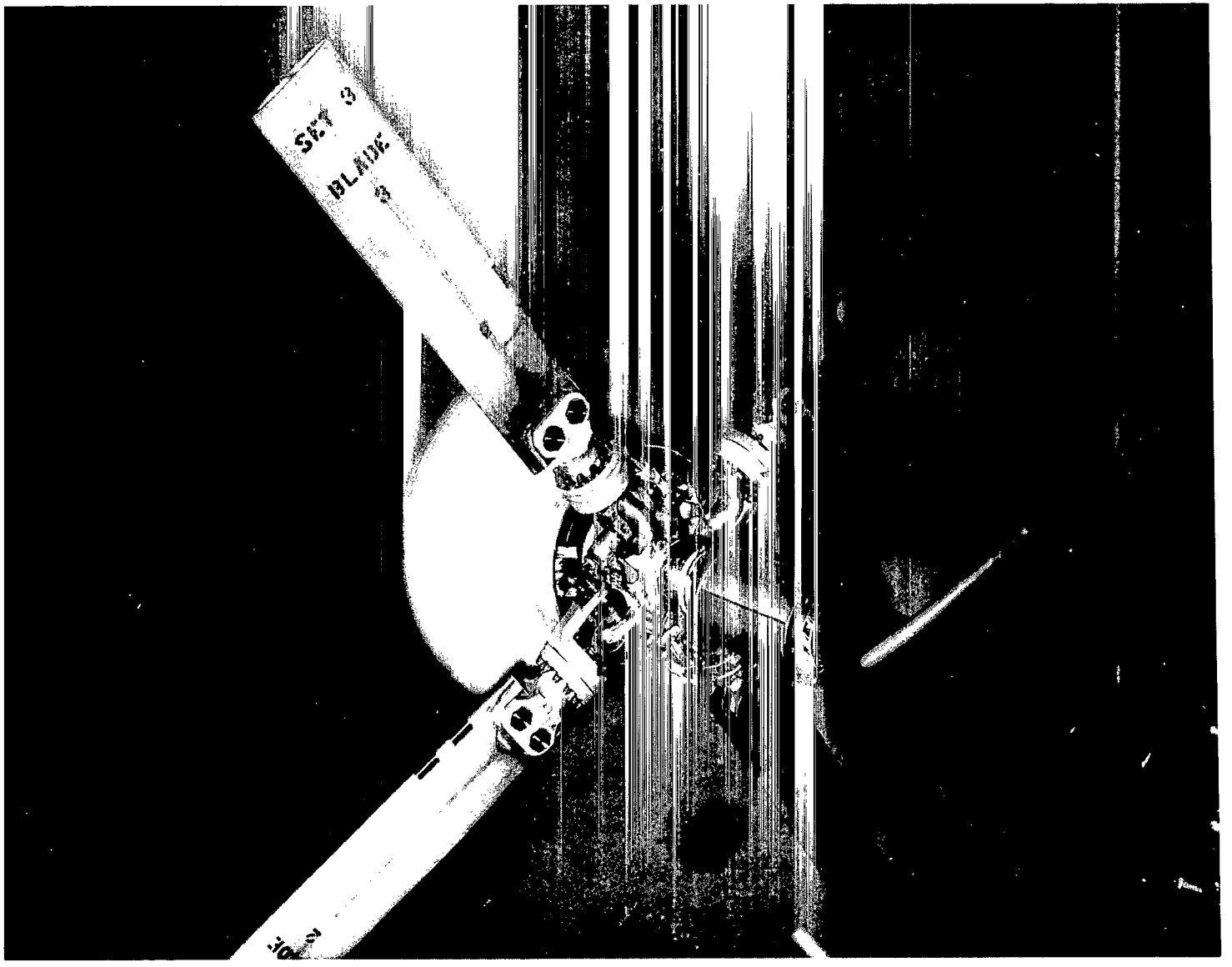

(a) Axial configuration; α = 61.5° to 90°

Figure 3.- Rotor entry vehicle mounted in the Ames 12-Foot Wind Tunnel.

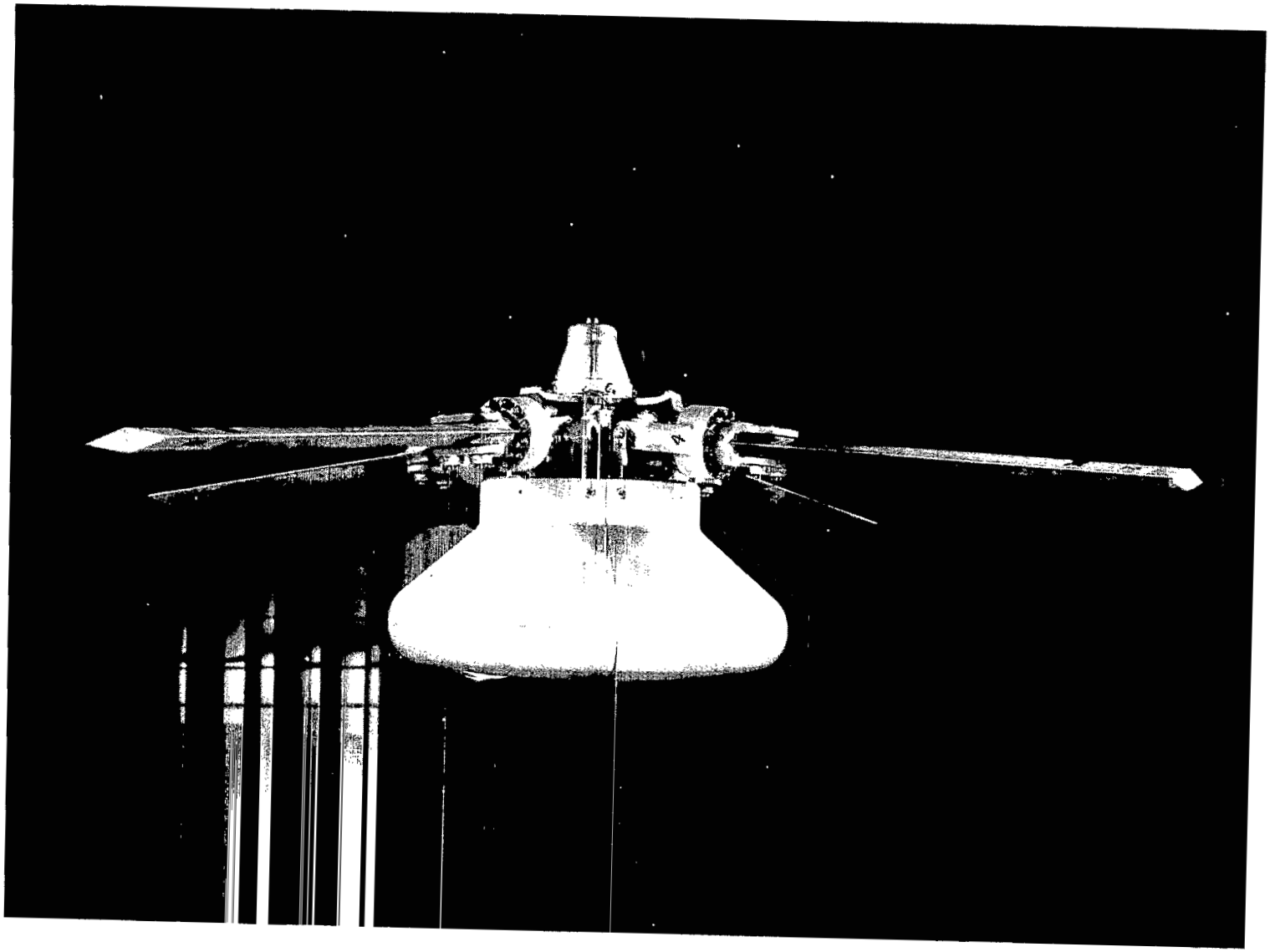

(b) Low angle configuration; $\alpha = 0^{\circ}$ to 28.5°

Figure 3.- Concluded.

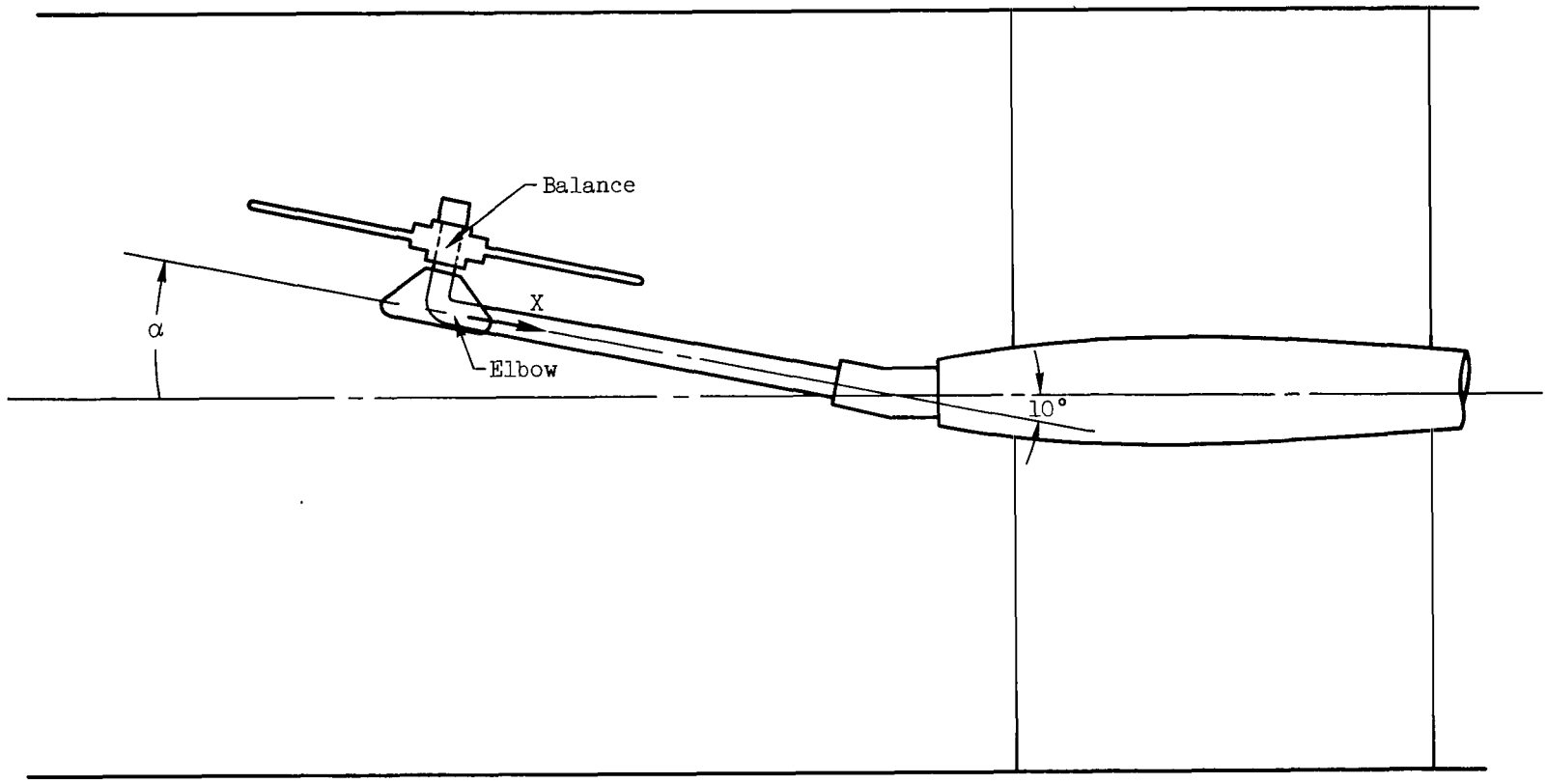

(a) $\alpha = 0^{\circ}$ to 28.5°

Figure 4.- Model mounting arrangements.

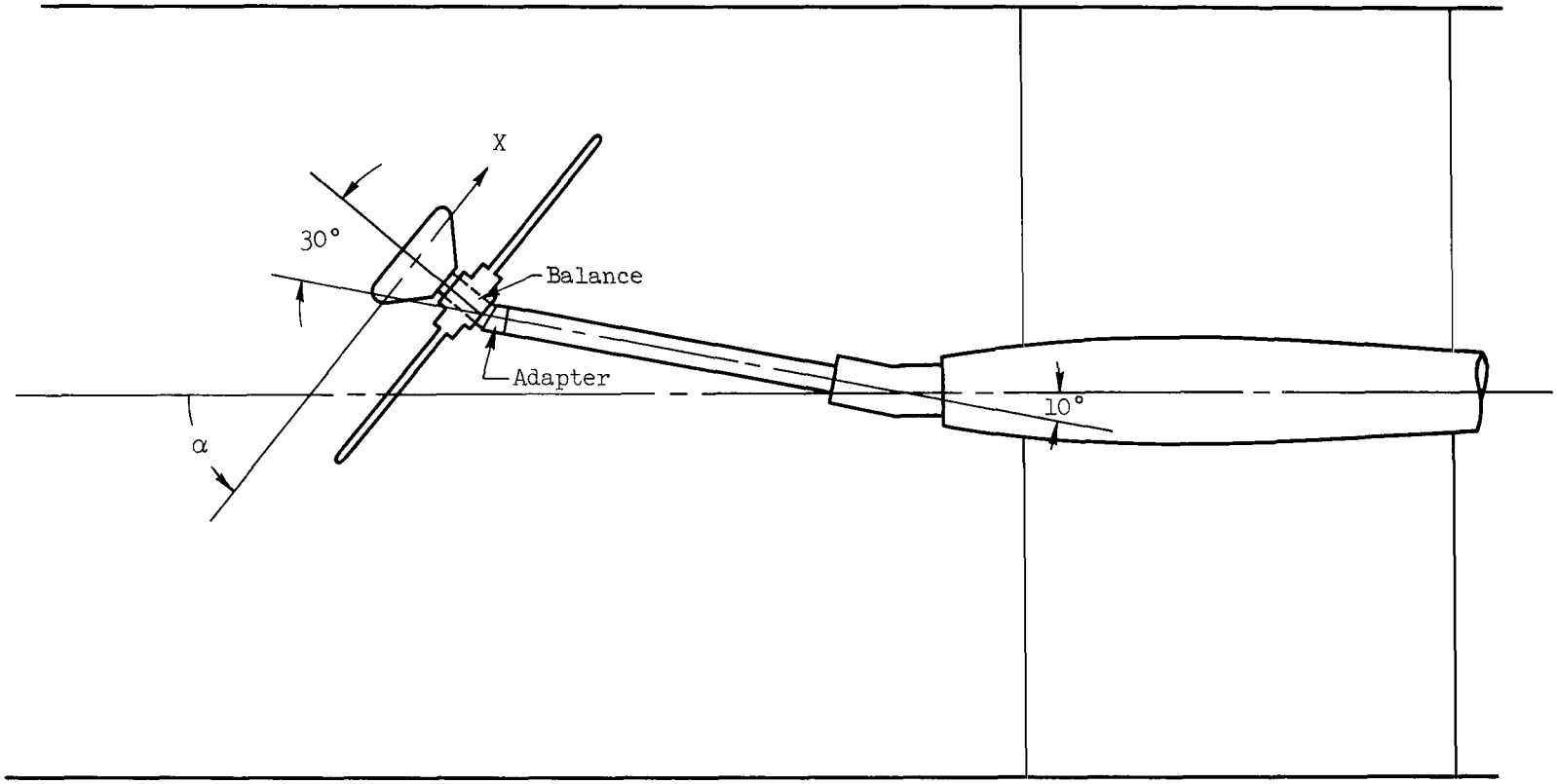

(b) $\alpha = 31.5^{\circ}$ to 60°

Figure 4.- Continued.

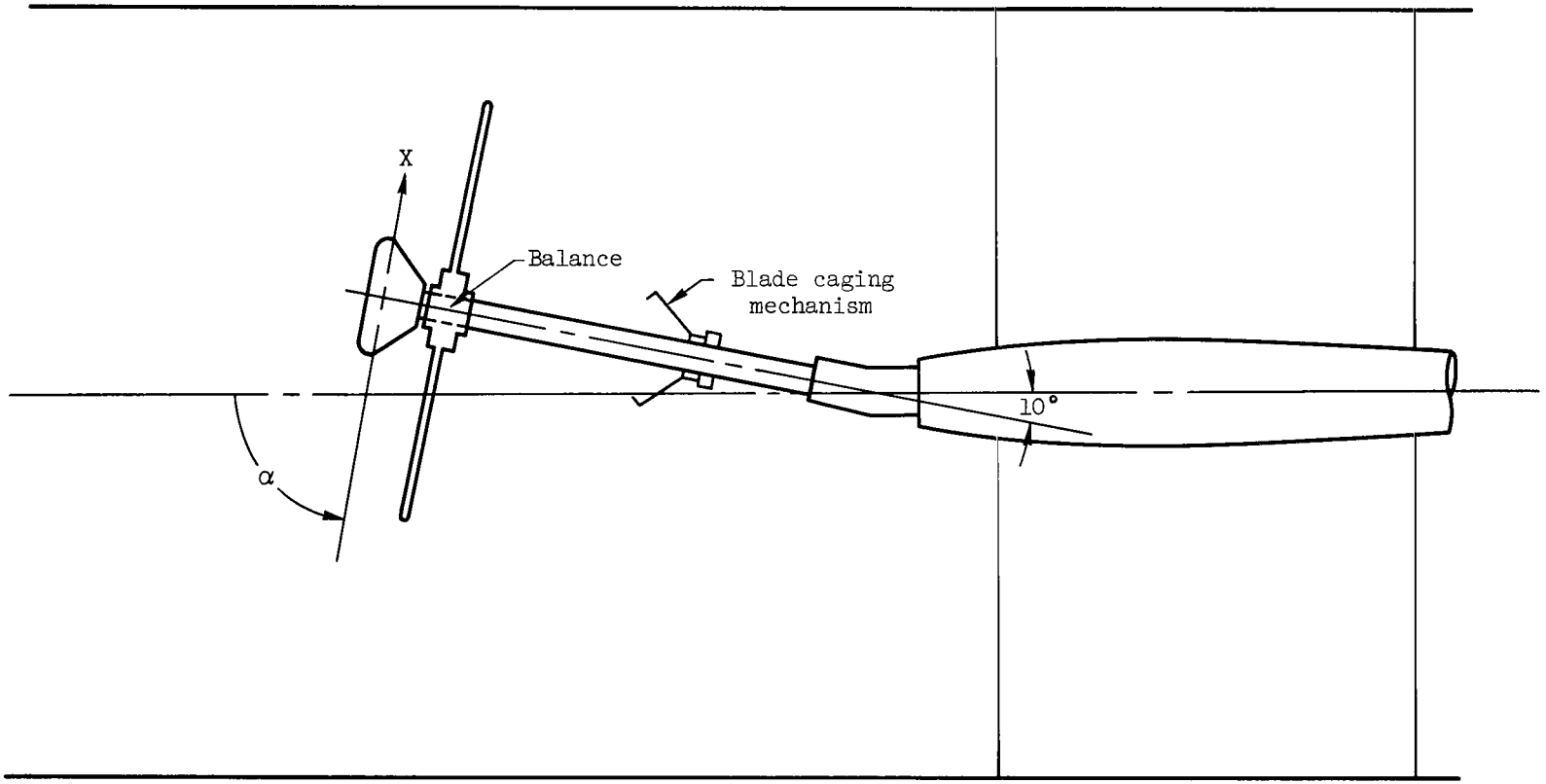

(c) $\alpha = 61.5^{\circ}$ to 90°

Figure 4.- Concluded.

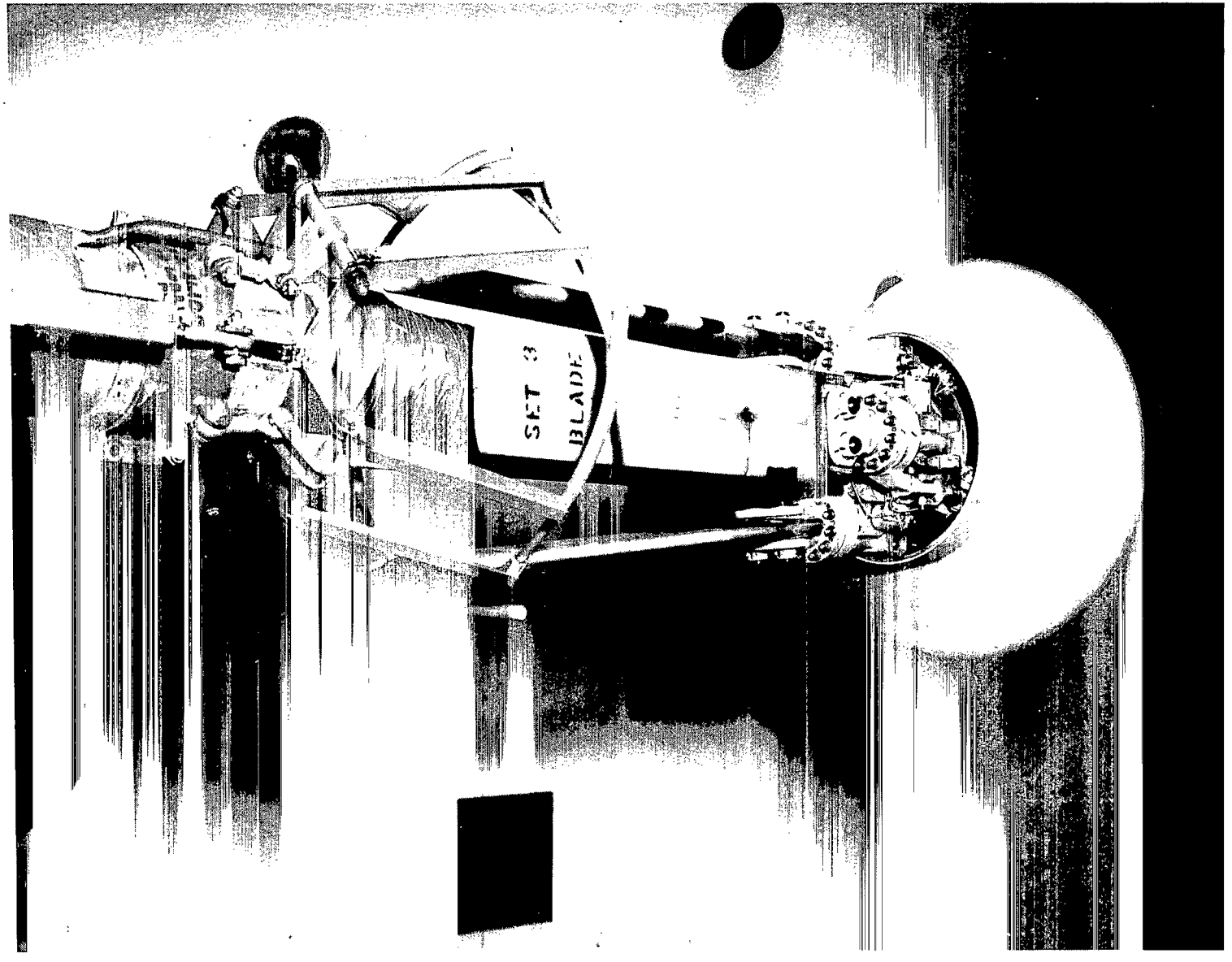

Figure 5.- Model with rotor blades in the caged position.

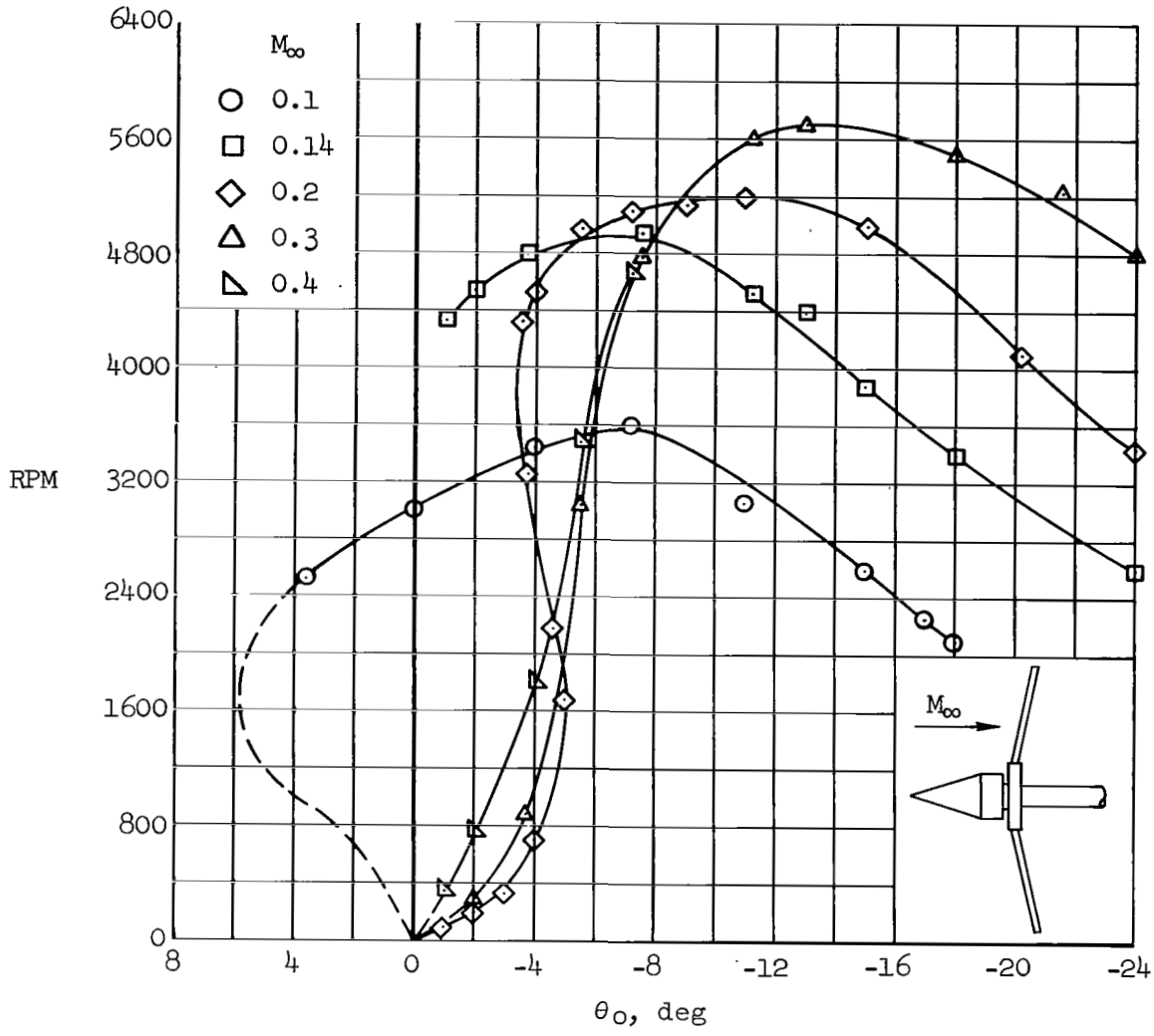

Figure 6.- Effect of stream Mach number on rotor speed for short elliptic-blade rotor with cone forebody; $\alpha = 90^o$.

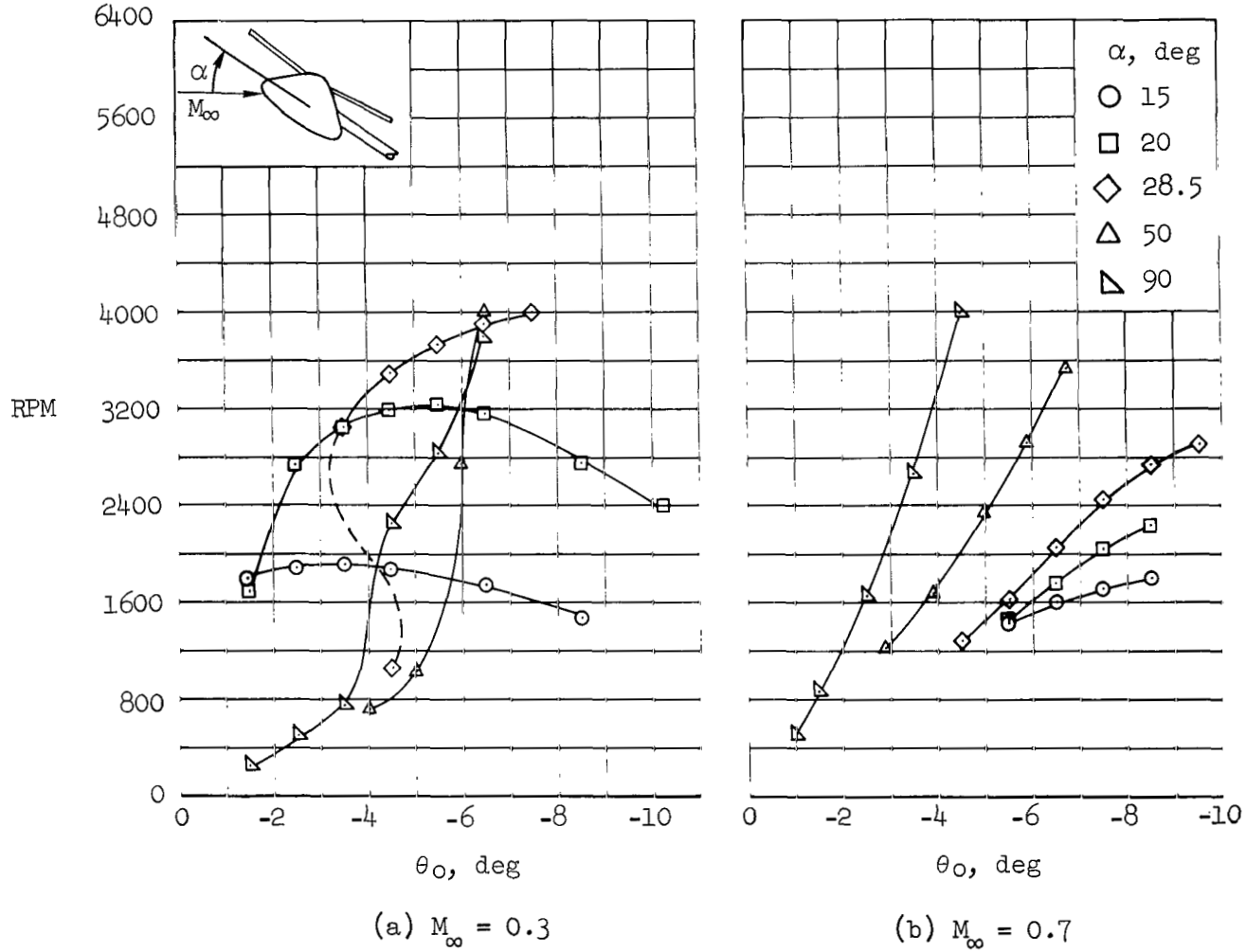

(a) $M_\infty = 0.3$ (b) $M_\infty = 0.7$

Figure 7.- Effect of angle of attack on rotor speed for short elliptic-blade rotor with capsule forebody.

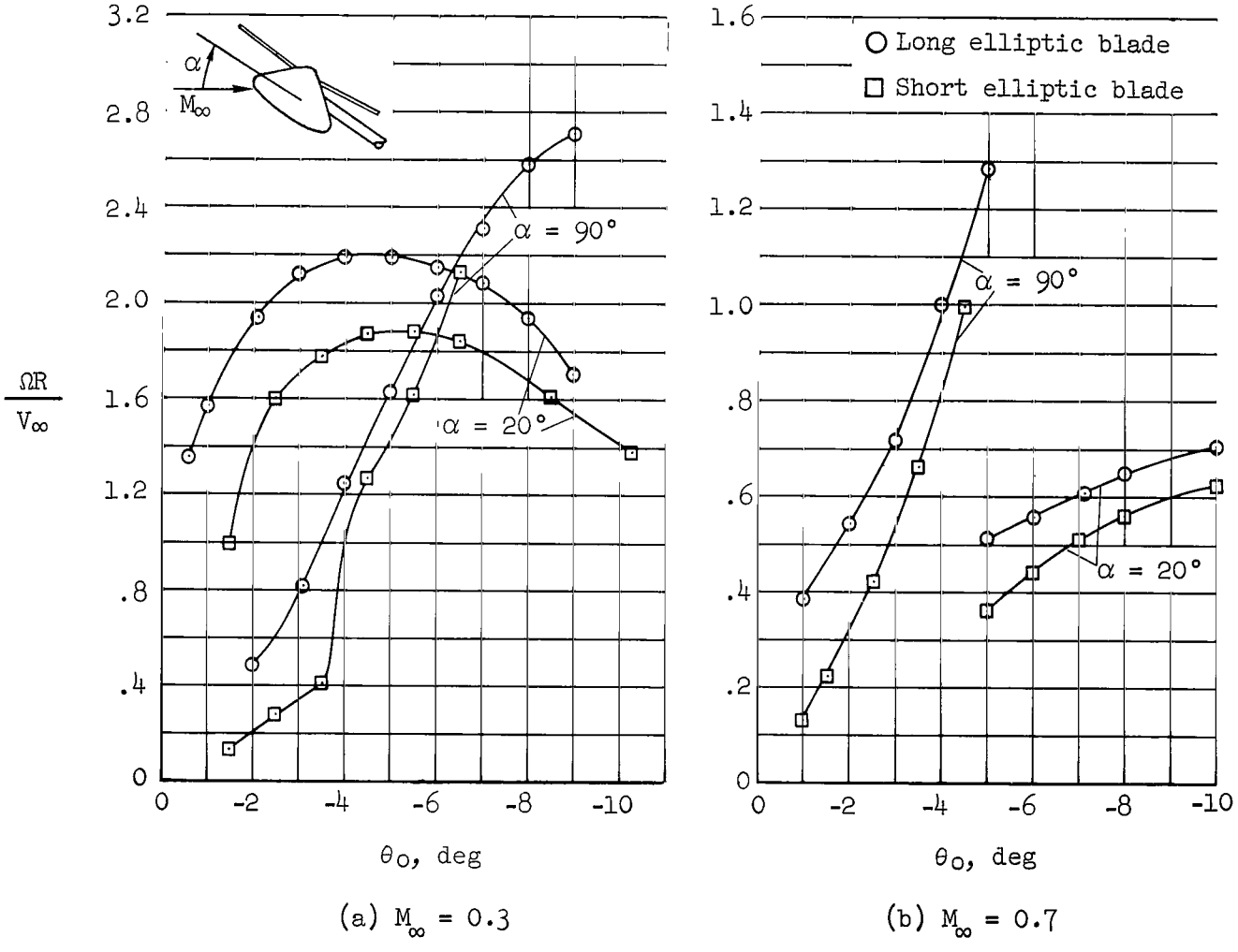

Figure 8.- Effect of blade length on rotor operating characteristics.

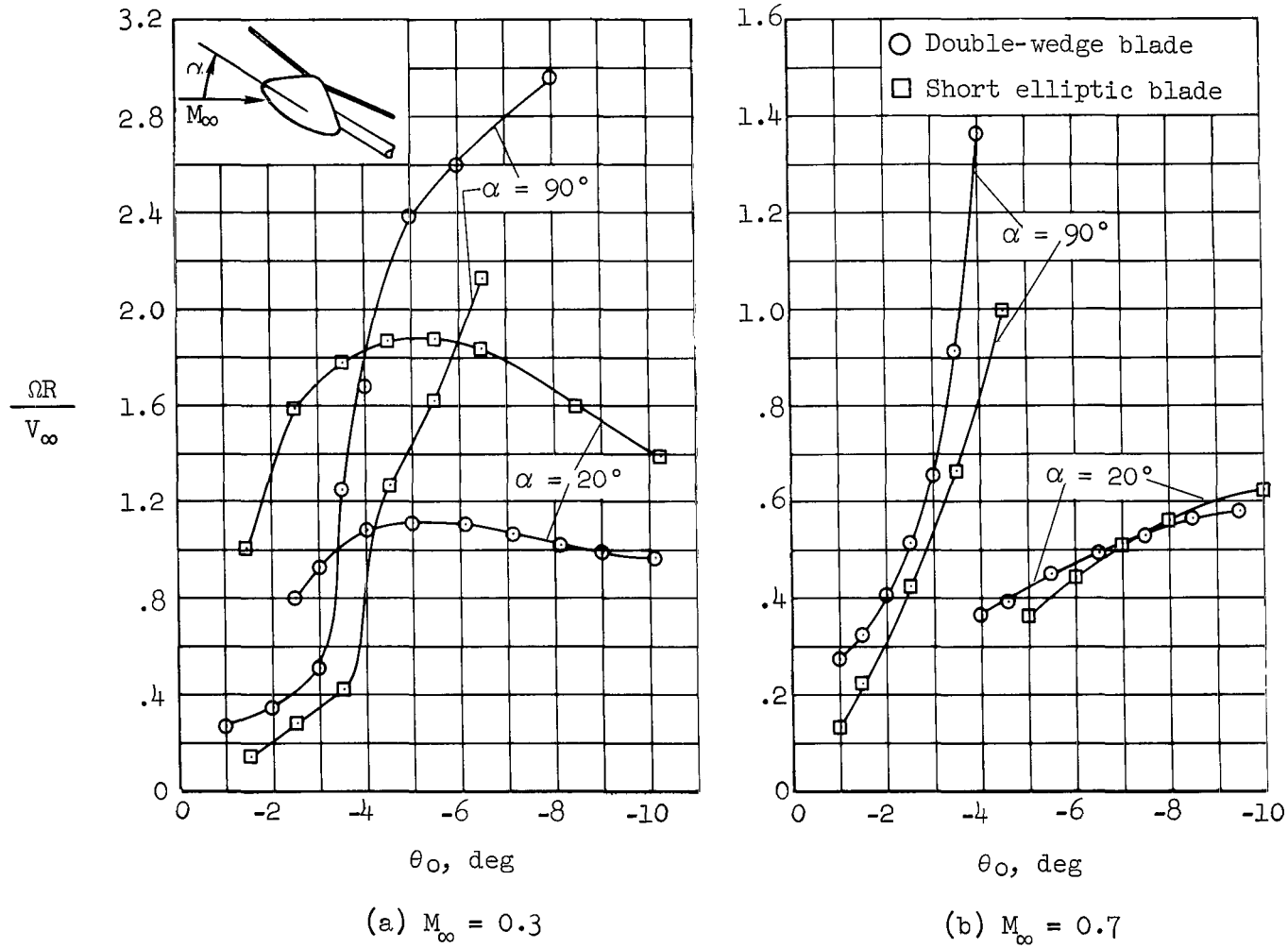

Figure 9.- Effect of blade section on rotor operating characteristics.

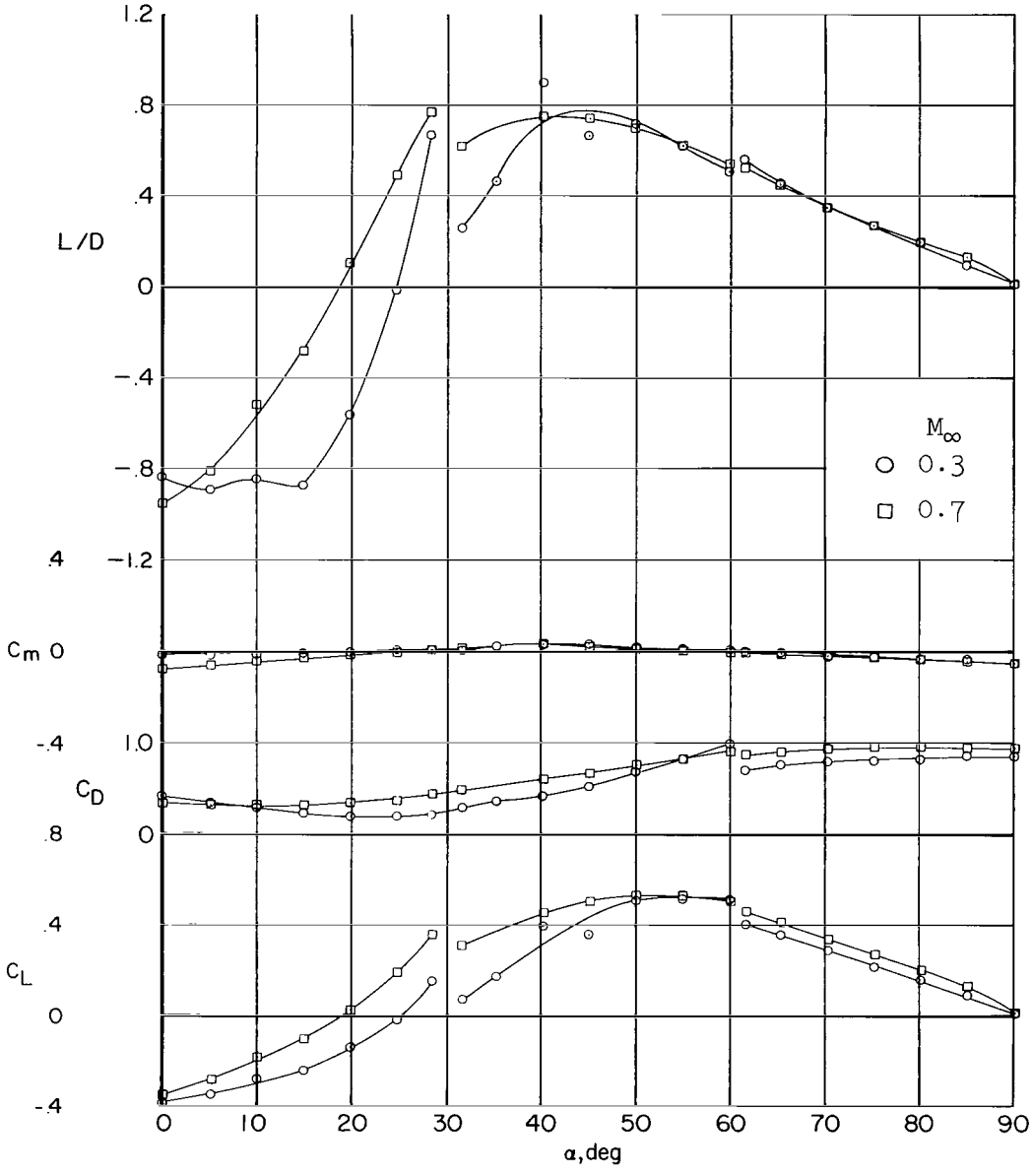

Figure 10.- Aerodynamic characteristics of the body alone.

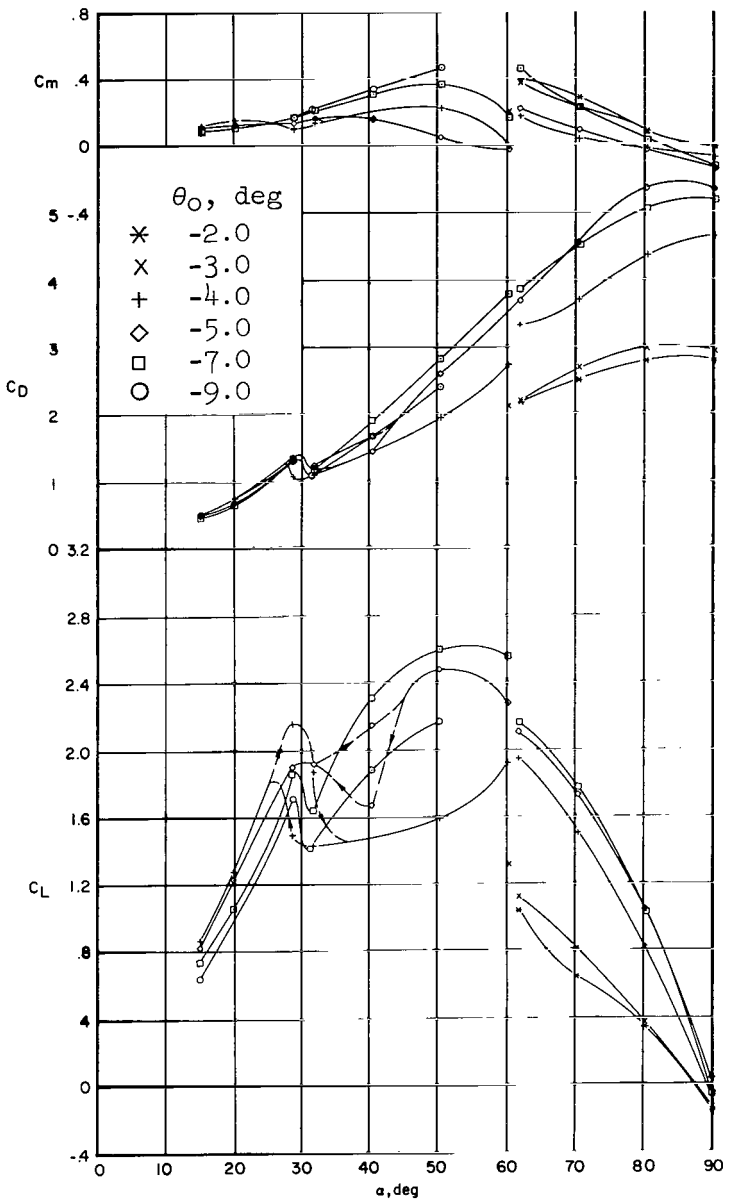

(a) $M_\infty = 0.3$

Figure 11.- Aerodynamic characteristics of the double-wedge blade configuration.

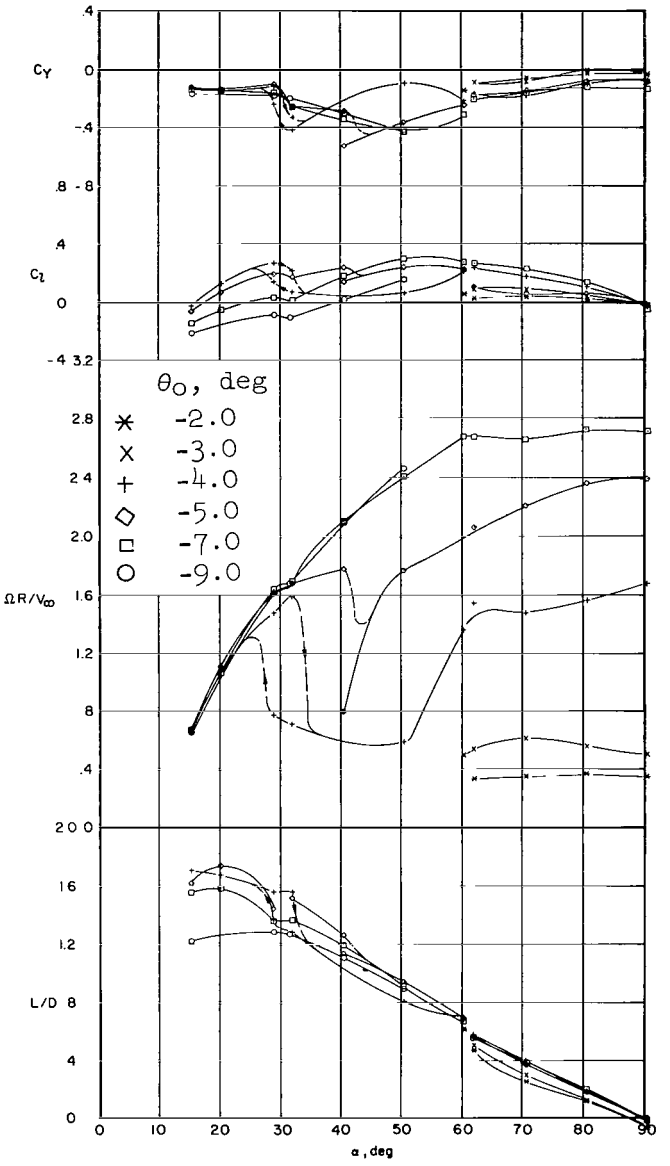

(a) M_∞ = 0.3 - Concluded.

Figure 11.- Continued.

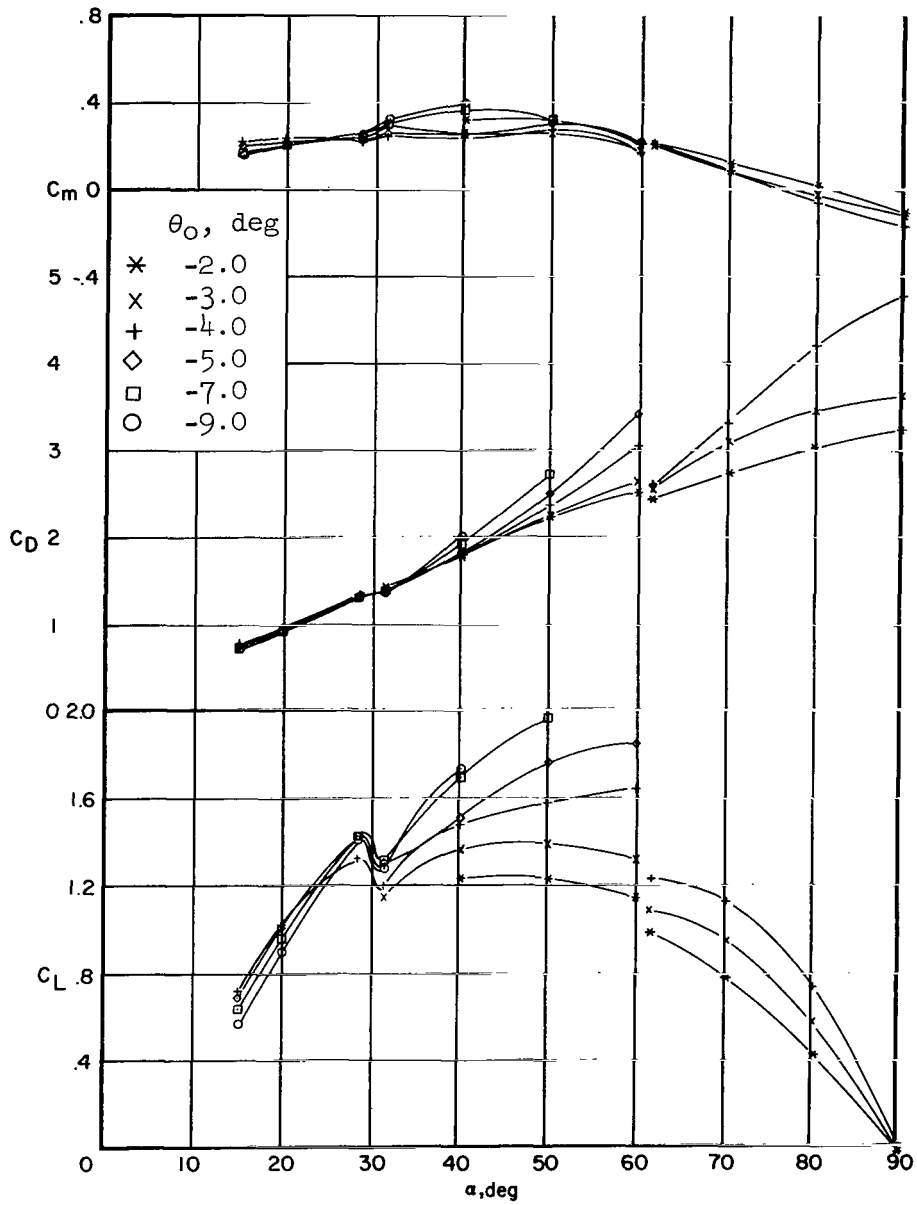

(b) $M_\infty = 0.7$

Figure 11.- Continued.

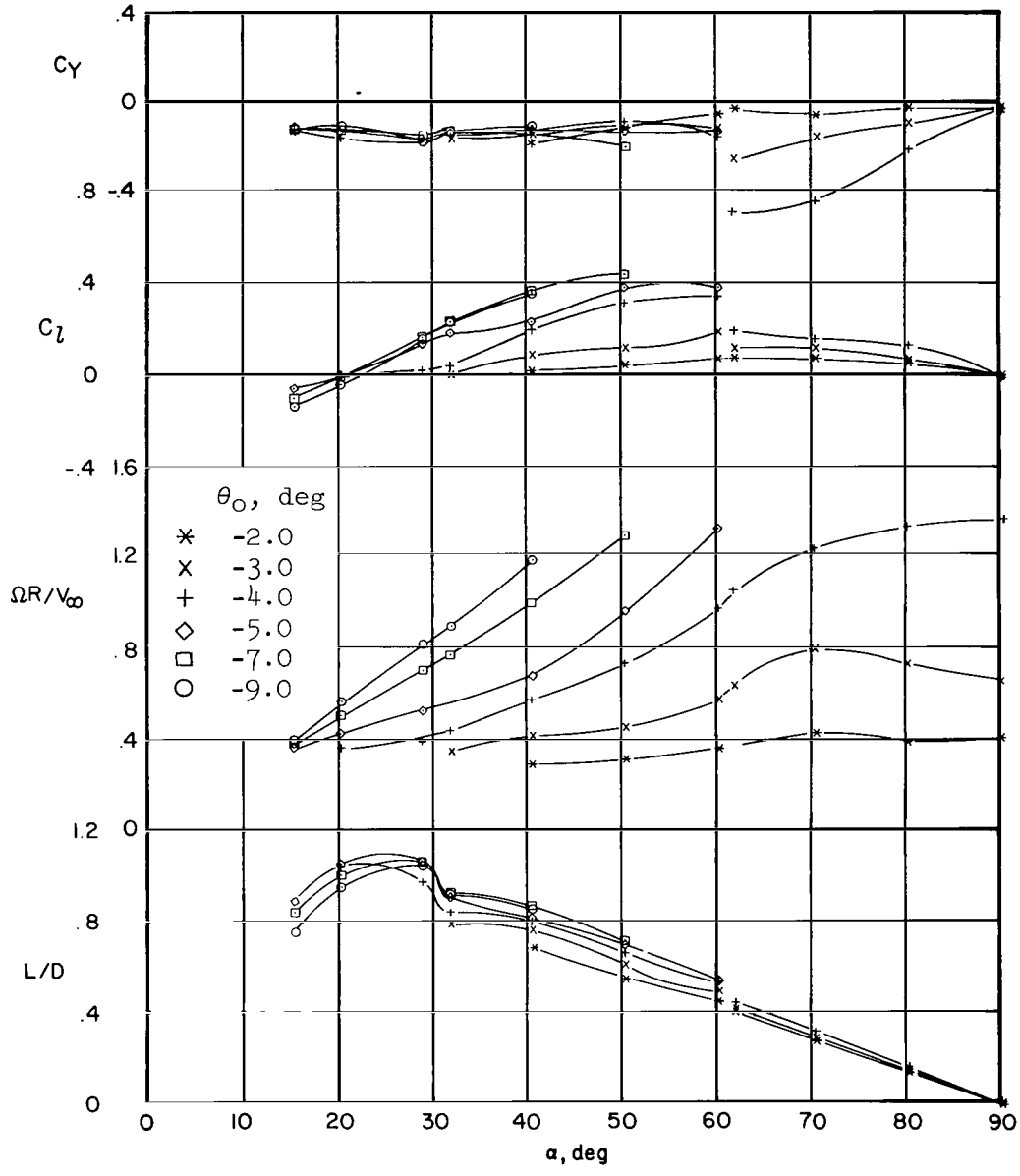

(b) M_∞ = 0.7 - Concluded.

Figure 11.- Concluded.

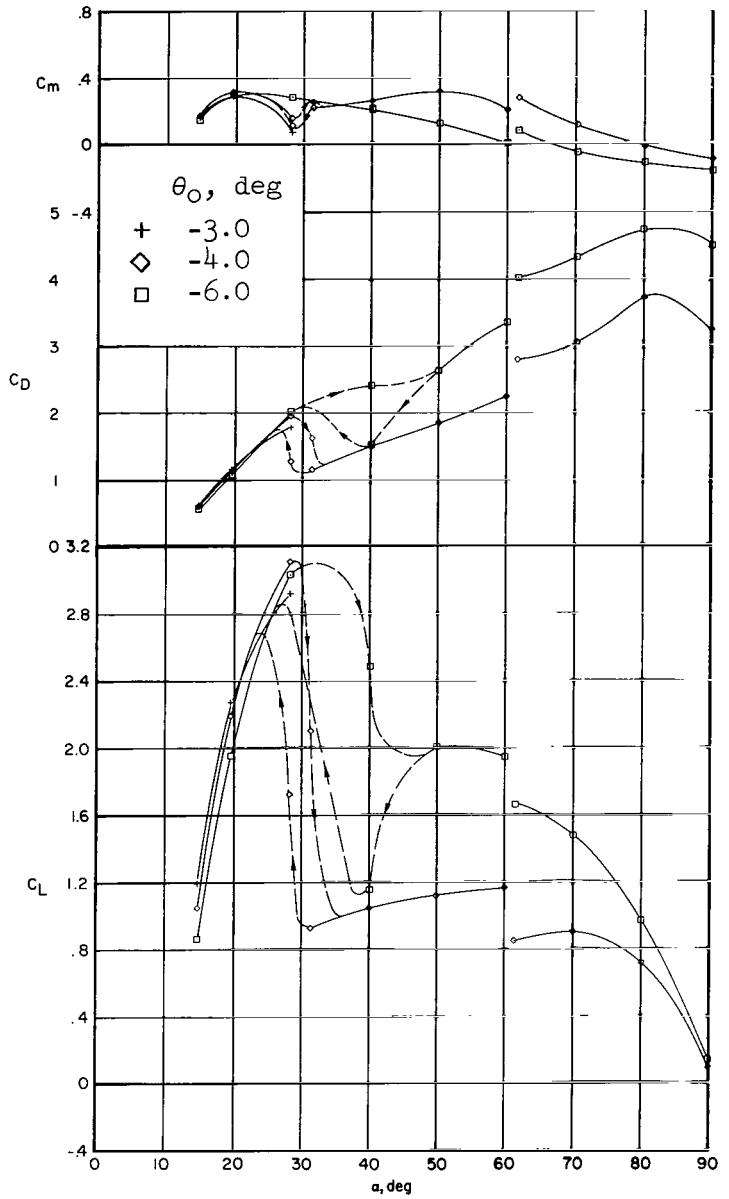

(a) $M_\infty = 0.3$

Figure 12.- Aerodynamic characteristics of the short elliptic-blade configuration.

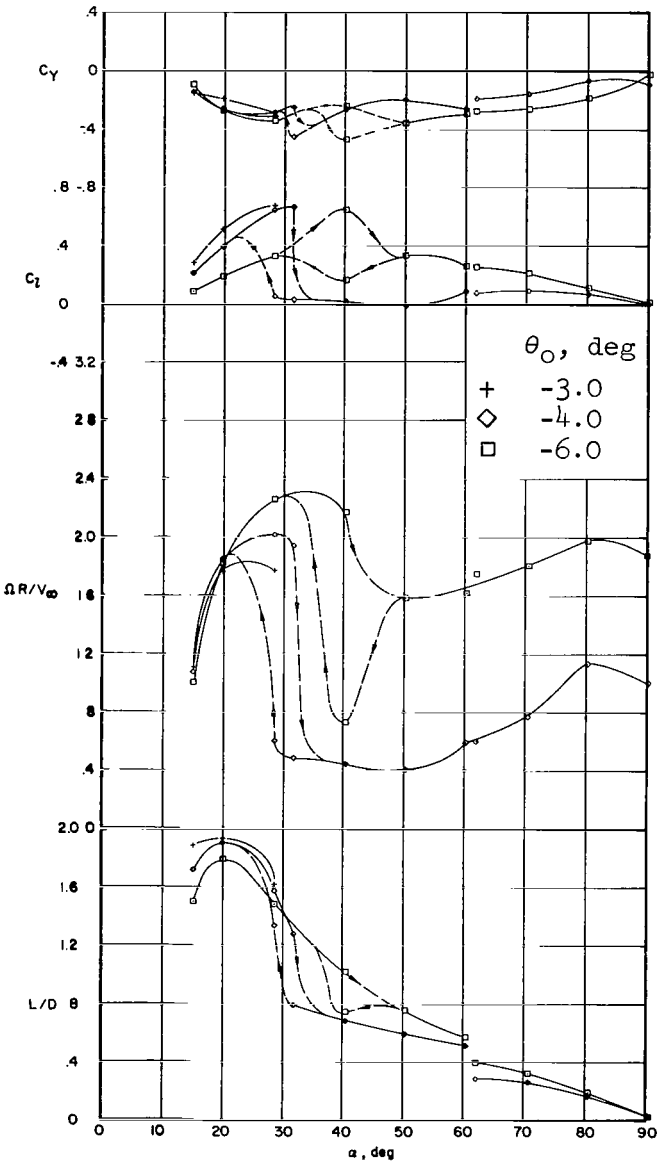

(a) M_∞ = 0.3 - Concluded.

Figure 12.- Continued.

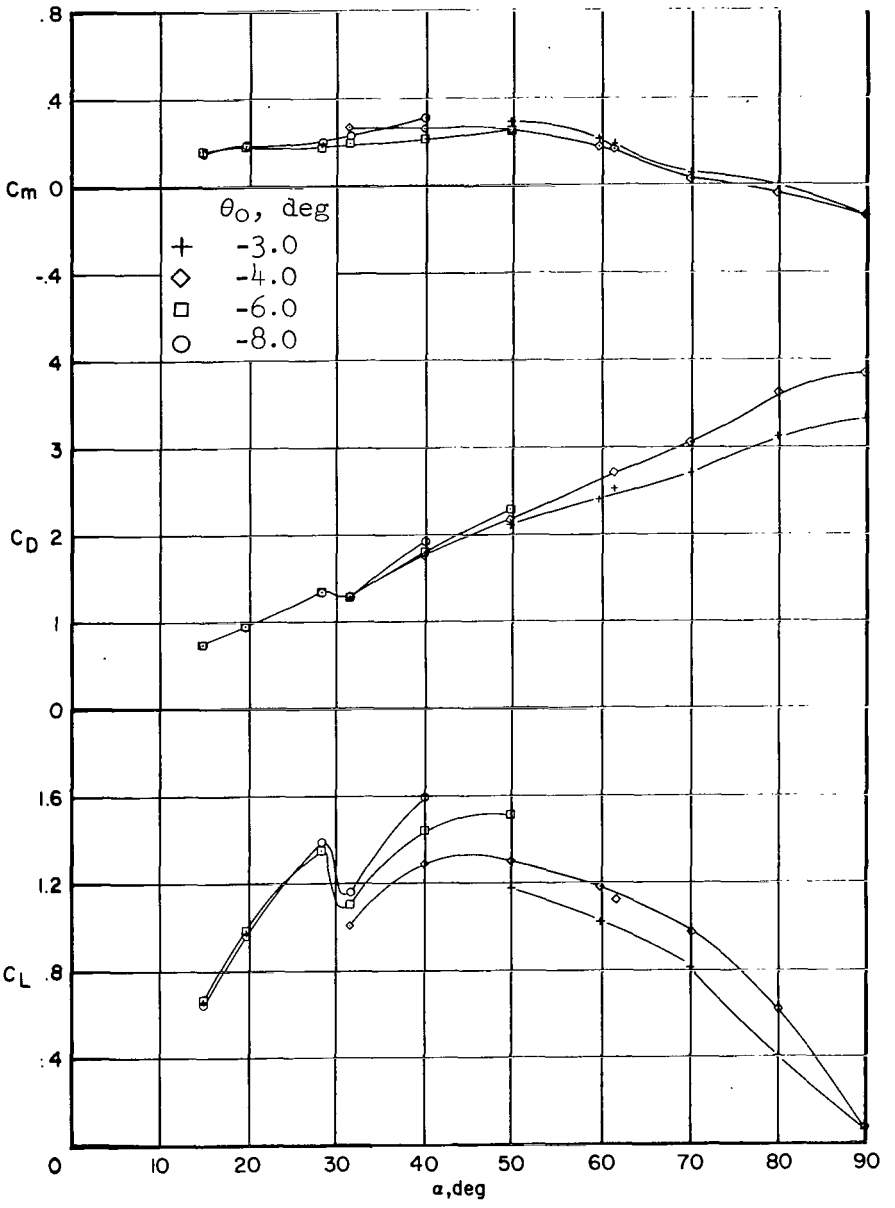

(b) $M_\infty = 0.7$

Figure 12.- Continued.

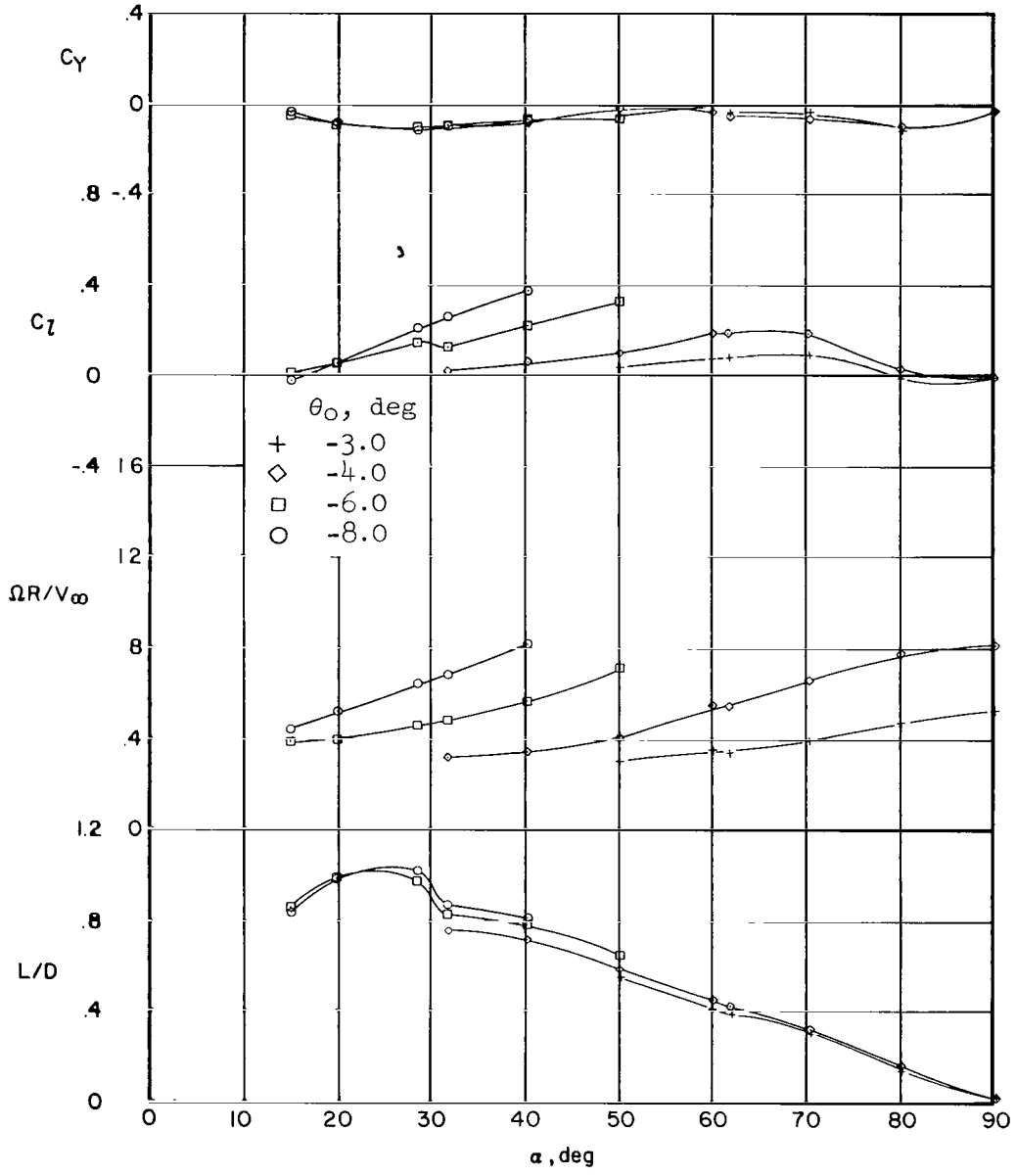

(b) $M_\infty = 0.7$ - Concluded

Figure 12.- Concluded.

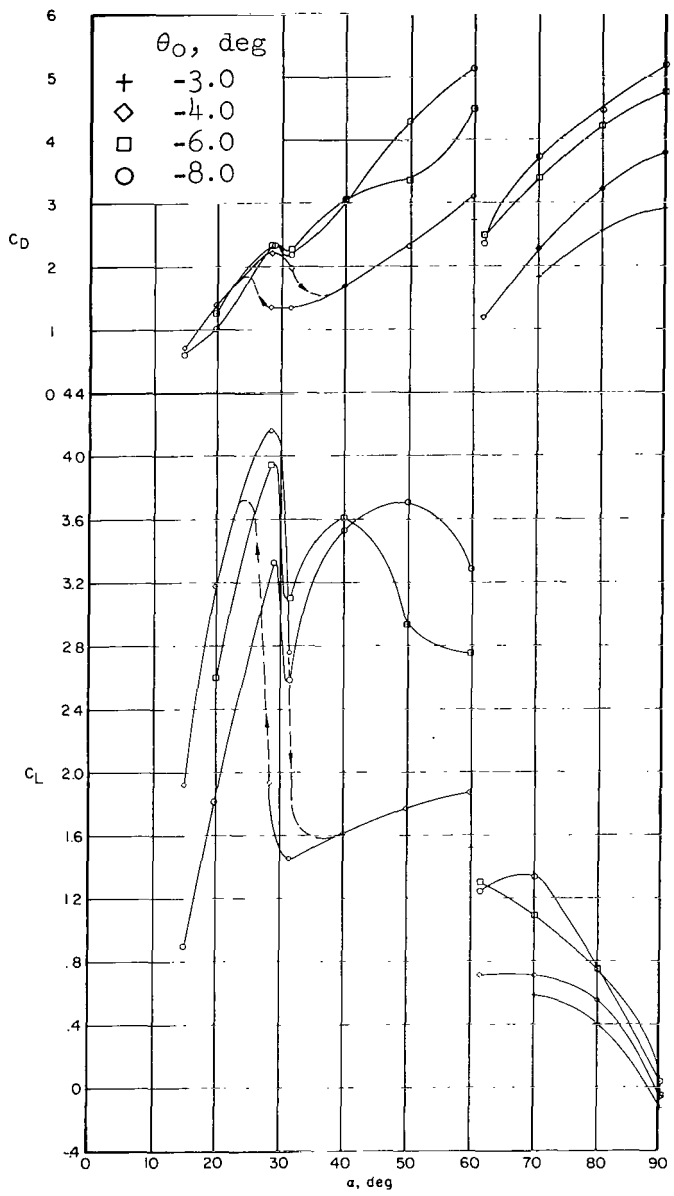

(a) $M_\infty = 0.3$

Figure 13.- Aerodynamic characteristics of the long elliptic-blade configuration.

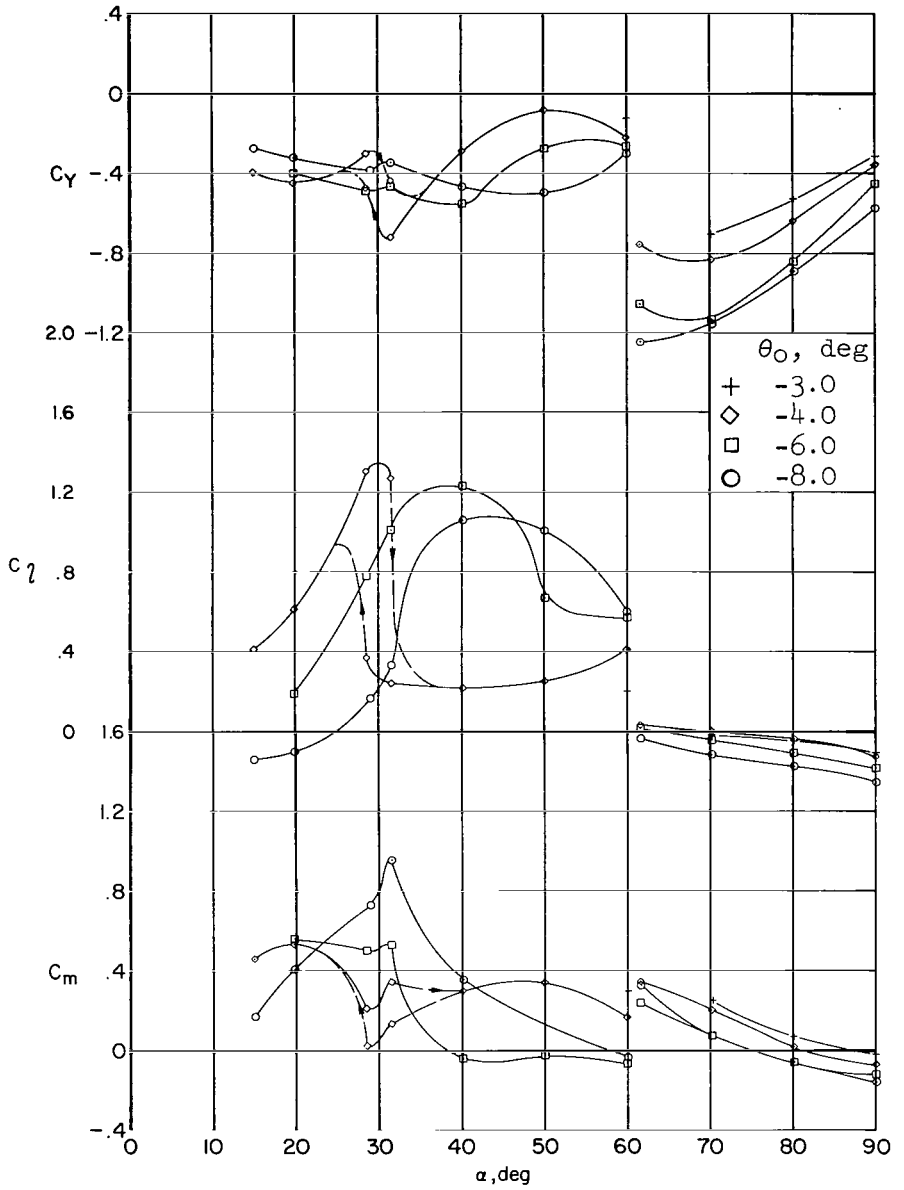

(a) M_∞ = 0.3 - Continued.

Figure 13.- Continued.

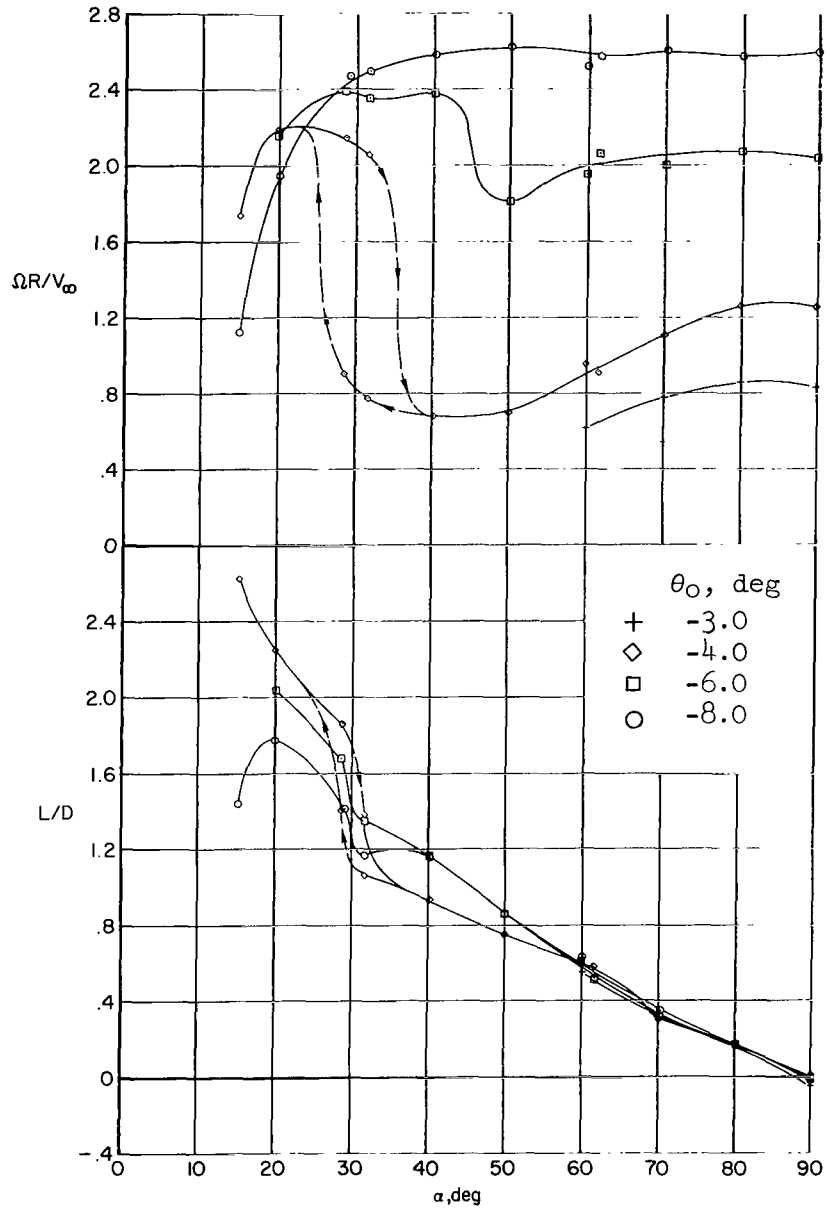

(a) M_∞ = 0.3 - Concluded.

Figure 13.- Continued.

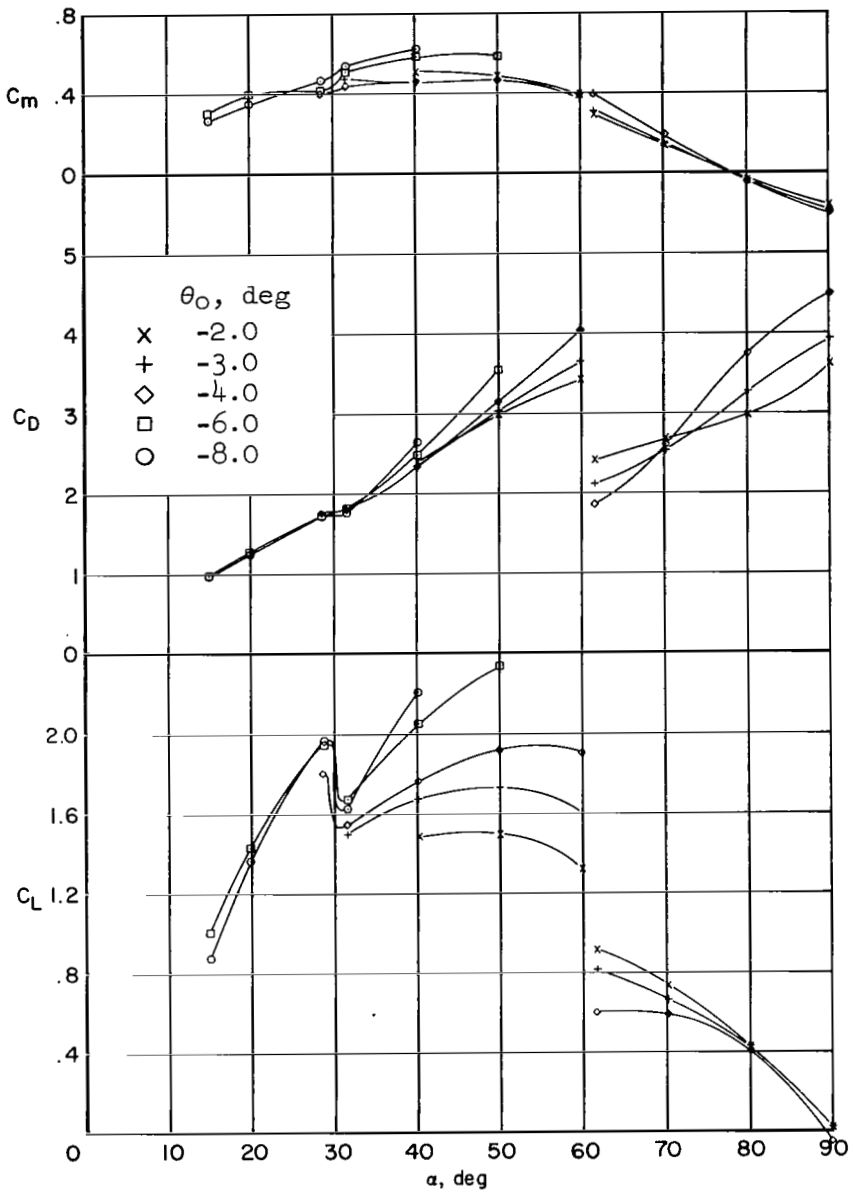

(b) $M_\infty = 0.7$

Figure 13.- Continued.

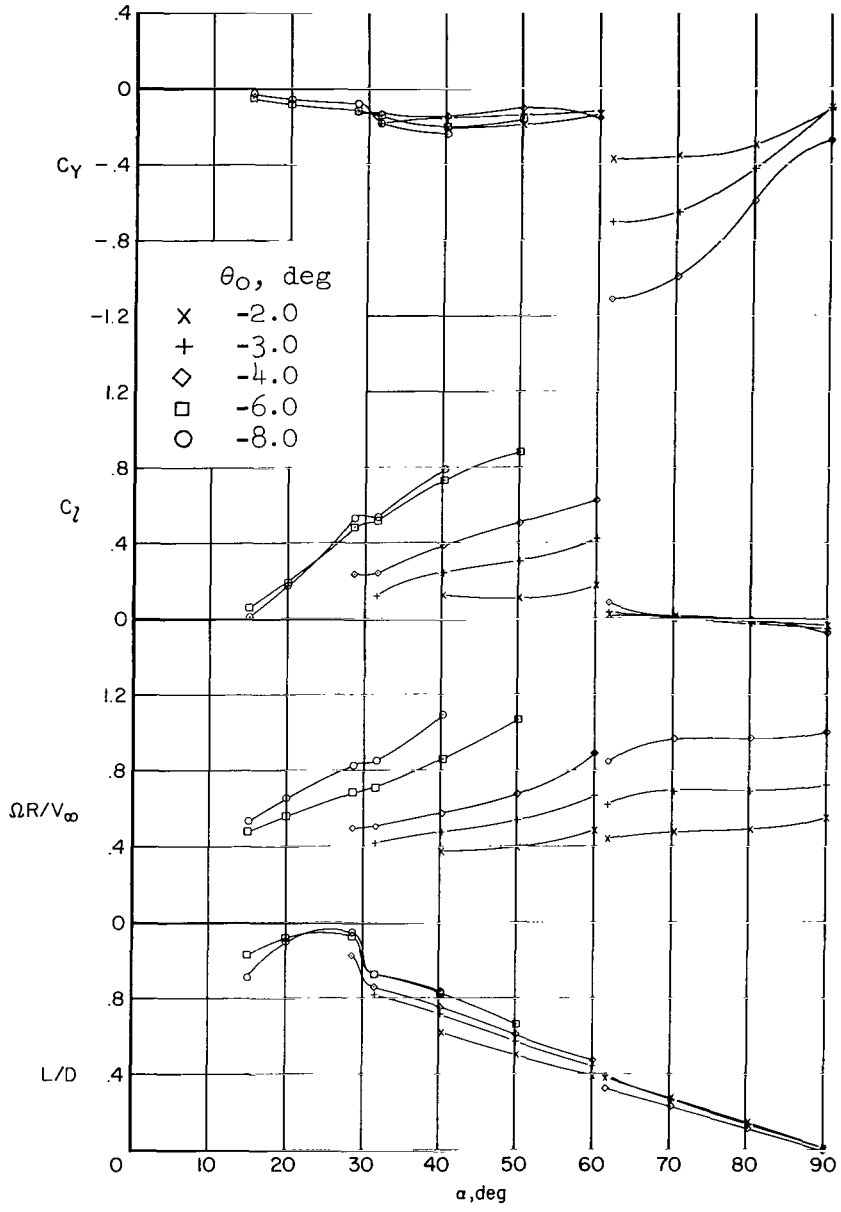

(b) M_∞ = 0.7 - Concluded.

Figure 13.- Concluded.

NASA-Langley, 1971 — 1 A-3709

"The aeronautical and space activities of the United States shall be conducted so as to contribute . . . to the expansion of human knowledge of phenomena in the atmosphere and space. The Administration shall provide for the widest practicable and appropriate dissemination of information concerning its activities and the results thereof."

—NATIONAL AERONAUTICS AND SPACE ACT OF 1958

NASA SCIENTIFIC AND TECHNICAL PUBLICATIONS

TECHNICAL REPORTS: Scientific and technical information considered important, complete, and a lasting contribution to existing knowledge.

TECHNICAL NOTES: Information less broad in scope but nevertheless of importance as a contribution to existing knowledge.

TECHNICAL MEMORANDUMS: Information receiving limited distribution because of preliminary data, security classification, or other reasons.

CONTRACTOR REPORTS: Scientific and technical information generated under a NASA contract or grant and considered an important contribution to existing knowledge.

TECHNICAL TRANSLATIONS: Information published in a foreign language considered to merit NASA distribution in English.

SPECIAL PUBLICATIONS: Information derived from or of value to NASA activities. Publications include conference proceedings, monographs, data compilations, handbooks, sourcebooks, and special bibliographies.

TECHNOLOGY UTILIZATION PUBLICATIONS: Information on technology used by NASA that may be of particular interest in commercial and other non-aerospace applications. Publications include Tech Briefs, Technology Utilization Reports and Technology Surveys.

Details on the availability of these publications may be obtained from:

SCIENTIFIC AND TECHNICAL INFORMATION OFFICE

NATIONAL AERONAUTICS AND SPACE ADMINISTRATION

Washington, D.C. 20546